Rush

Journal Title: Journal of Petrology

Volume: 33
Issue: 2
Month/Year: 1992
Pages: 423-469

Article Author: Ernst and Bell

Article Title: Petrology of the Great abtibi Dyke, Superior Province, Canada

Imprint:

Account #: 83767800

Location:

Item #:

CUSTOMER HAS REQUESTED:
Mail to Address

Laurent Montesi (01271)
MS 24
Woods Hole, MA 02543

Email: lmontesi@whoi.edu
Electronic Delivery? Yes

0022-3530/92 $3.00

Petrology of the Great Abitibi Dyke, Superior Province, Canada

by RICHARD E. ERNST[1] AND KEITH BELL[2]

[1]*Ottawa–Carleton Geoscience Centre and Department of Geology, University of Ottawa, Ottawa, Ontario, Canada K1N 6N5*

[2]*Ottawa–Carleton Geoscience Centre and Department of Earth Sciences, Carleton University, Ottawa, Ontario, Canada K1S 5B6*

(*Received 21 March 1991; revised typescript accepted 27 August 1991*)

ABSTRACT

The Great Abitibi Dyke (GAD) which can be traced northeast, for >700 km, across the Abitibi Belt in the southeastern Superior Province of the Canadian Shield, is composed of olivine gabbro to monzodiorite, weakly saturated to undersaturated in silica.

All rocks of the GAD can be derived by mainly plagioclase and olivine fractionation from a parental magma corresponding in composition to chilled margin samples. Two units can be distinguished, a marginal unit (Unit 1) representing 0–50% crystallization and a central unit (Unit 2), found over about half of the dyke length, representing 50–70% crystallization. Modelling, using Pearce elemental ratio analysis, quantifies the fractionation history and allows mass-balance calculations over the present exposure level of the dyke. The approximate balance between the amounts of cumulate and fractionated rocks suggests that Unit 1 differentiated essentially *in situ* as a closed system. In contrast, Unit 2 rocks were formed by loss of substantial plagioclase and olivine from the parental magma. This fractionate must have either been lost to depth or left behind in an external chamber. Unit 2 rocks show depletion in plagioclase and enrichment in mafic minerals along strike towards the southwest (deeper exposure level?), a trend explained by density stratification. Regional variation in Unit 1 chemistry is interpreted in terms of lateral magma injection towards the northeast from the locus of Keweenawan rift volcanism. Feldspar, olivine, and augite compositions are linearly correlated with equilibrium temperature and extent of magma evolution.

The parent magma had a trace element chemistry corresponding to a 'within-plate' setting and was probably derived from an incompatible-element enriched mantle similar to the source for ocean island basalts (OIBs).

INTRODUCTION

Dykes are the primary mode of mafic magma transport through the crust and knowledge of their emplacement and differentiation histories is therefore important for understanding the controls on magma migration. Detailed studies of large dykes are few but among those studied are the 400 km long Cleveland dyke of the British Tertiary Province (Macdonald *et al.*, 1988) and a mid-Proterozoic dyke of similar length in Greenland (Kalsbeek & Taylor, 1986). The present study adds to the emerging database on mafic mega-dykes and provides a detailed petrogenetic study of the Great Abitibi Dyke, one of the largest in Canada.

The Great Abitibi Dyke (GAD) can be traced for at least 700 km across the Abitibi belt, southeastern Superior Province, Canadian Shield, from the Kapuskasing Structural Zone (KSZ) to the Grenville Front (Fig. 1). The GAD, the most prominent member of the Abitibi swarm, has a U–Pb age of 1140·6±2 Ma (Krogh *et al.*, 1987). Although significantly younger than the Archean host terrane, the dyke is similar in age to rocks of the Keweenawan rift system, located to the southwest in the Lake Superior basin, and to many

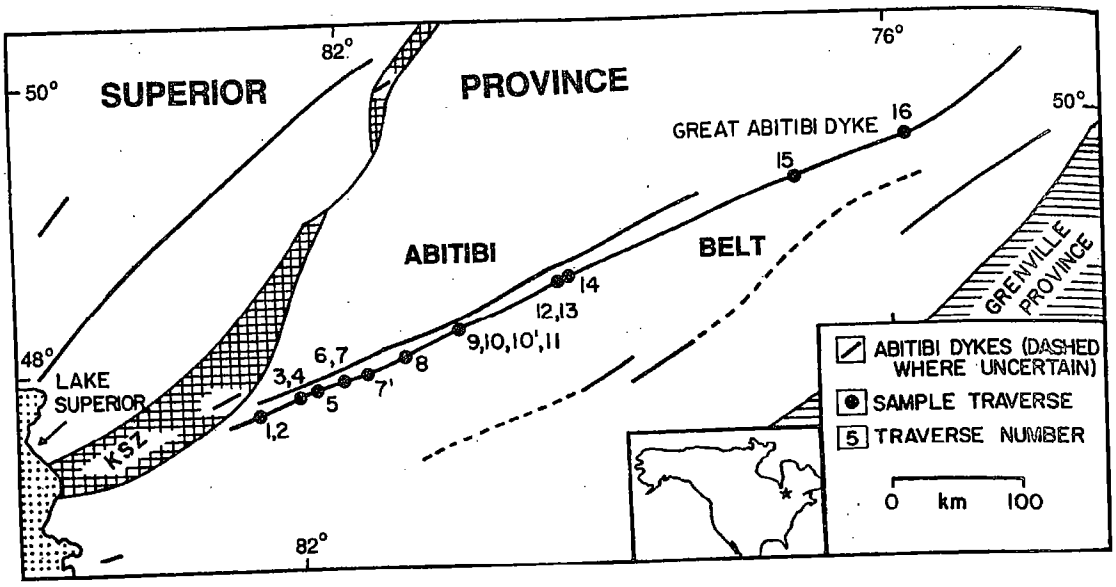

FIG. 1. Regional setting of the Abitibi dyke swarm [modified from Fahrig & West (1986) and Ernst *et al.* (1987)] and sampling sites.

carbonatites in the Superior Province (e.g., Bell & Blenkinsop, 1987; Ernst *et al.*, 1987). Emplacement of the GAD and the rest of the Abitibi swarm has been related to a stress field caused by boundary loads associated with the Grenville Orogeny (Ranalli & Ernst, 1986).

The unmetamorphosed GAD is continuous along most of its length except in its mid-length portion where it breaks into en echelon segments with offsets up to 1 km (Ernst, 1991). The GAD varies in thickness from 80 m up to 250 m and is thickest along its mid-length portion (Ernst *et al.*, 1987). Metre-wide mini-dykes branch off the main dyke at a number of traverses. Previous reconnaissance studies of the Abitibi swarm (e.g., Goodwin *et al.*, 1972; Card *et al.*, 1981; Condie *et al.*, 1987) indicate that the dykes (including the GAD) are gabbroic in composition, characteristically contain olivine and have a distinctive chemistry including a weakly alkaline character and light rare earth element (LREE) enrichment.

This paper details the petrology of the Great Abitibi Dyke and evaluates its emplacement and differentiation history.

FIELD AND PETROGRAPHIC OBSERVATIONS

The Great Abitibi Dyke (GAD), studied at 16 traverses spaced along 550 km of its length (Fig. 1), shows aphanitic chilled margins that contain micro-phenocrysts of plagioclase and more rarely of olivine. Grain size ranges up to very coarse grained and rock types consist of gabbro, diorite, and monzodiorite. [Grain size classes follow Williams *et al.* (1982); fine is <1 mm, medium is 1–5 mm, coarse is 5–30 mm and very coarse is >30 mm.] Plagioclase, augite, olivine, titanomagnetite, and ilmenite are the most abundant minerals; accessory minerals include alkali feldspar, apatite, and biotite; and trace minerals include baddeleyite and zircon. The dyke consists of multiple phases which most prominently divide the dyke into two units, an outer unit (Unit 1) and an axial central unit (Unit 2). Unit 2 extends from between traverses 4 and 5 to between traverses 14 and 15. Units 1 and 2 were initially distinguished on the basis of whole-rock chemical composition (described below). However, these two units also differ in rock and mineral textures as well as in mineral chemistry.

Field observations

Unit 1 rocks can be distinguished from those of Unit 2 in the field using textural criteria. Unit 1 rocks (aphanitic to coarse grained) normally have a random fabric, whereas Unit 2 rocks (coarse to very coarse grained) are commonly characterized by an igneous lamination defined by tabular plagioclase grains. Unit 1 can be subdivided at some traverses (e.g., traverse 7) into an outer (1a) and inner (1b) unit (Fig. 2), marked by changes in grain size across the contact, and mafic pegmatites locally intruded along contact planes (Fig. 3). Unit 1a rocks are also cut by irregular fine-grained mini-dykes (0·5–2 m wide), probably belonging to Unit 1b, that locally contain xenoliths of Unit 1a rocks. There are slight modal differences between the two sub-units; rocks of Unit 1a typically contain <35% mafic minerals, whereas Unit 1b rocks average 40%.

The transition from Unit 1 to Unit 2 rocks (best seen at traverse 7) is marked by a gradual change from a subophitic to an intergranular texture and by the development of a weak igneous lamination in Unit 2 defined by tabular plagioclase grains. Unit 2 rocks at traverse 7 contain about 50% (by volume) of mafic minerals and also wispy, discontinuous mafic zones (Fig. 3C) which roughly parallel the feldspar lamination and some feldspathic zones. Although most outcrops of Unit 2 exhibit a weak feldspar lamination, only at traverse 7 was the exposure sufficient to map the pattern of lamination which defines a synform with a subhorizontal axis trending northeast, i.e. parallel to the trend of the dyke. The laminated zone of the south limb of the synform is broader than that on the north limb, and the trough (Fig. 2) is shifted slightly northwards from the centre-line of the dyke. Such asymmetries are consistent with the dyke-dip having been off-vertical (70–80°S; Ernst, 1991) during crystallization of Unit 2 magma. The absence of a similar pattern in Unit 1 rocks may be due to its faster cooling rate which allowed less time for mass transfer under gravity across the inclined dyke.

Mafic mini-dykes (<2 m wide), similar in composition to Unit 1 rocks, trend subparallel to the GAD, and at traverses 2, 5, 7, 9, 13 and 14 they cut the adjacent host rocks; at traverse 4 they intrude the GAD.

The chilled margins of the main dyke and the mini-dykes contain up to 10% tabular plagioclase phenocrysts (maximum length 1 cm) generally aligned parallel to the contacts. Smaller olivine crystals are occasionally present.

The contact relationships observed at traverse 7 (Fig. 4), and probably applicable to all parts of the dyke, indicate that Unit 1a was intruded by Unit 1b which in turn, was intruded by Unit 2. The lack of any chilled samples or mini-dykes of Unit 2 composition at any traverses along the complete length of the dyke suggests that Unit 2 developed *in situ* or was emplaced while Unit 1b rocks were still hot and ductile thus providing an easy pathway for magma injection down the centre of the dyke.

Petrography

In Unit 1 rocks, plagioclase is typically intergrown with olivine, and both minerals are partially enclosed by anhedral augite. Olivine occurs both as isolated grains and as grain aggregates. Alkali feldspar is interstitial. These textural observations constrain the relative order in which mineral phases enter the liquidus. The order is: plagioclase and olivine together, followed by both apatite and the iron–titanium oxides, and finally followed by both augite and alkali feldspar.

In rocks of Unit 2, subhedral plagioclase, olivine, and augite define an intergranular texture and represent an orthocumulate with plagioclase, olivine, and augite as cumulus phases. Olivines typically enclose apatite and iron–titanium oxides. Alkali feldspar (anorthoclase) occurs as overgrowths on embayed plagioclase and also occurs interstitially. These

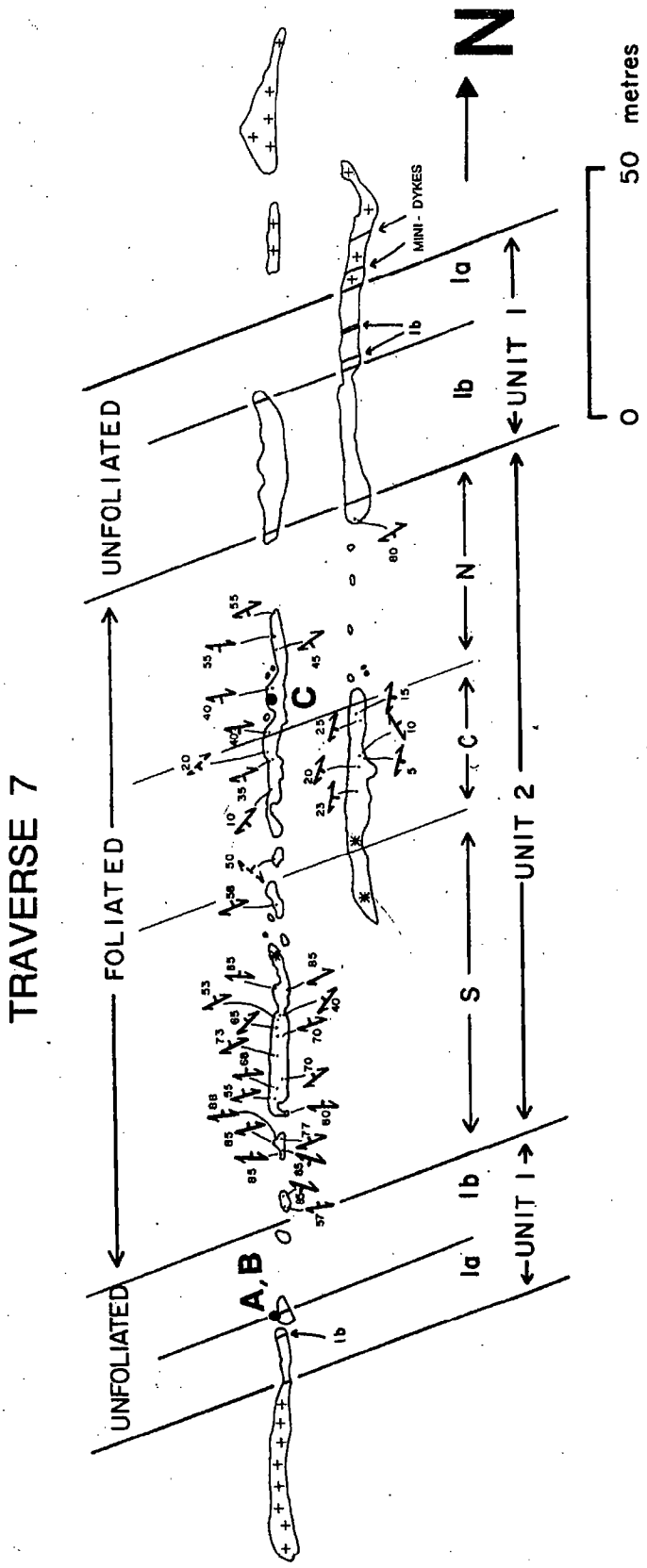

FIG. 2. Outcrop map (plan view) at traverse 7, showing subdivisions of the dyke, and the orientations of feldspar laminations in Unit 2 rocks. Outcrops of granitoid host rock are marked by crosses. Unit 1 is subdivided into Units 1a and 1b. Unit 2 is subdivided on the basis of the dip of the feldspar lamination into three groups, north (N), central (C), and south (S). The two 'dashed' symbols indicate approximate measurements. The asterisk locates where the feldspar grains have random orientation. Capital letters and large dots indicate the position of photographs shown in Fig. 3.

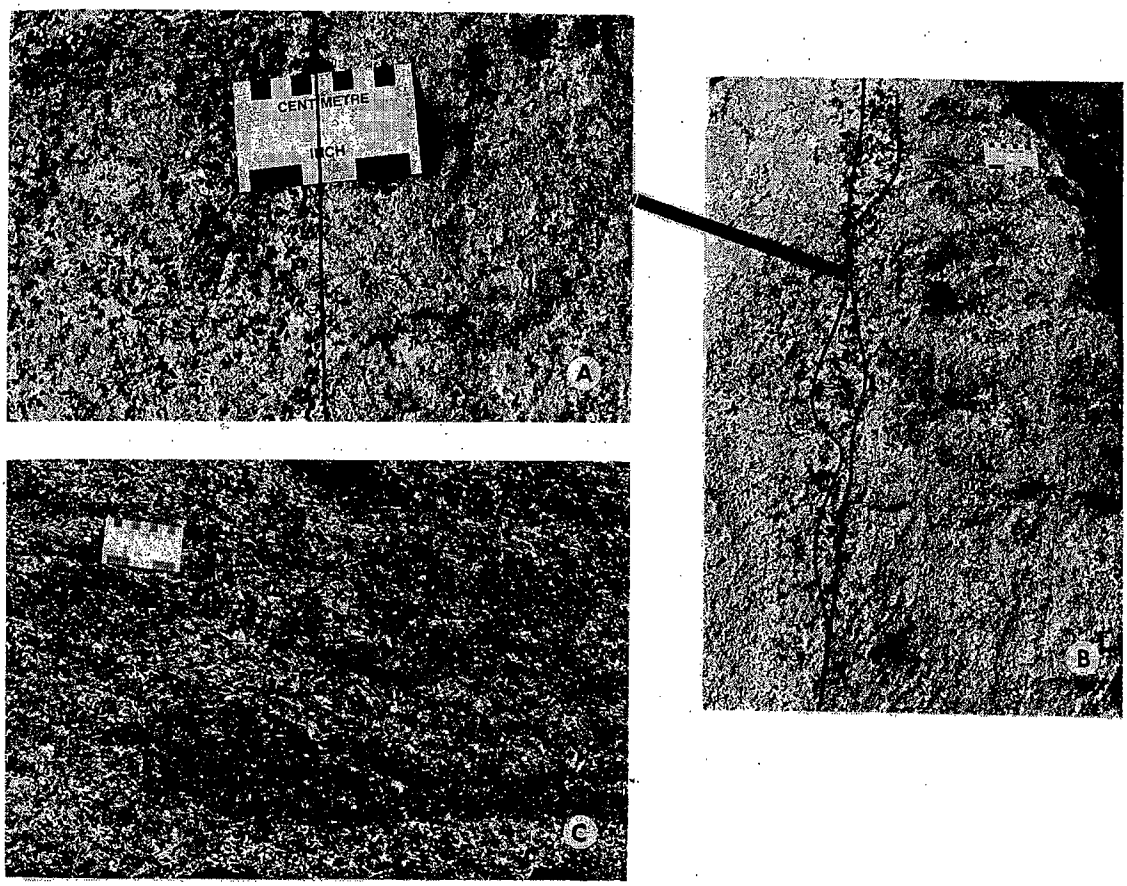

FIG. 3. Photographs taken in the field at traverse 7. (See Fig. 2 for photo locations.) (A) is located at the contact between Units 1a (left side) and 1b (right side). (B) shows a larger field of view of the same area and shows the presence of a local pegmatitic phase along the contact between Units 1a and 1b. [Internal contacts in (A) and (B) have been inked for greater clarity.] The contacts are diffuse, but Unit 1b is fine-grained in contact with medium-grained rock of Unit 1a. (C) shows rock of Unit 2 in the dyke interior. The light mineral is mainly plagioclase (with minor alkali feldspar), and the dark minerals include augite, olivine, and Fe–Ti oxides. Two textural features are of special note in (C): feldspar grains are tabular with a preferred orientation defining a lamination parallel to the long dimension of the photograph; and there are mafic streaks with long axes parallel to the feldspar lamination.

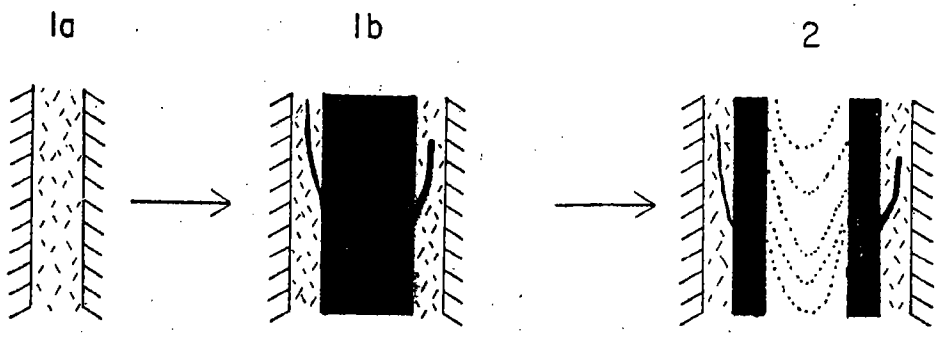

FIG. 4. Cross-sections at traverse 7 after emplacement of Unit 1a, 1b, and 2, respectively. Unit 1a rocks have random dashed pattern, Unit 1b rocks are in solid black, and Unit 2 are marked by U-shaped dotted lines. Host rock indicated by ruled pattern.

textural observations suggest that the order in which the mineral phases began to accumulate is as follows: first, apatite and iron–titanium oxides, followed by both augite and olivine, then plagioclase, and finally by both alkali feldspar and biotite.

Ilmenite in both Units 1 and 2 occurs as: (1) isolated, anhedral grains; (2) irregularly shaped regions in the cores of anhedral titanomagnetite grains (composite grains; Morse, 1980); and (3) exsolution lamellae in anhedral titanomagnetite crystals. Iron–titanium oxides are commonly rimmed by biotite. In both Units 1 and 2, apatite occurs as acicular to prismatic euhedral crystals up to 0·5 mm in size.

Modal compositions were determined by point-counting (generally 1000 points per sample) and results are summarized in Table 1. Although the modal abundances are highly variable throughout the sample suite, Units 1 and 2 have similar average total feldspar, olivine, augite, titanomagnetite, apatite, and biotite contents and differ only in the proportion of alkali feldspar to plagioclase. On the basis of relative proportions of plagioclase, clinopyroxene, and olivine (Streckeisen, 1976), most Unit 1 rocks can be classified as olivine gabbros. Unit 2 rocks contain alkali feldspar exceeding 10% of the total feldspar present, and have plagioclase of composition $An_{<50}$. Therefore, Unit 2 rocks should be classified as monzodiorites on the basis of the Q–A–P–F diagram (Streckeisen, 1976).

Nepheline and other feldspathoids were not observed, and orthopyroxene was found in only three samples (one from an altered chilled margin at traverse 10 and two others from the southwest end of Unit 2 at traverse 5). The virtual absence of both nepheline and orthopyroxene suggests that the GAD magma remained transitional between silica-saturated and silica-undersaturated conditions throughout its differentiation history.

MINERAL CHEMISTRY

The composition of feldspar, olivine, augite, titanomagnetite, and ilmenite, as well as some trace alteration minerals, were determined by quantitative wavelength-dispersive analysis

TABLE 1

Average modal compositions of Units 1 and 2

	Unit 1			*Unit 2*		
	n	x̄	*S.D.*	n	x̄	*S.D.*
Plagioclase	29	60·8	7·6	13	44·2	10·5
Alkali feldspar	29	2·2	2·4	13	13·0	6·1
Total feldspar	30	62·9	6·3	14	57·2	10·8
Olivine	30	10·3	5·9	14	7·0	4·0
Augite	30	14·3	6·6	14	19·8	6·7
Fe–Ti oxides*	30	7·6	2·7	14	7·0	2·3
Apatite	30	2·4	1·6	14	3·5	1·1
Biotite	30	1·7	1·0	13	3·6	2·2
Orthopyroxene	30	0·0	—	14	0·0	—
Nepheline	30	0·0	—	14	0·0	—
Other†	21	0·6	0·5	12	2·0	1·9

n, number of samples analyzed. One thin-section was point-counted per sample.
x̄, average percentage modal abundance.
* Ilmenite is typically more abundant than titanomagnetite.
† 'Other' includes minor primary minerals such as baddeleyite and zircon as well as deuteric or secondary minerals such as amphibole, chlorite, prehnite, and pectolite. Trace sulphides are sometimes present.

using a Cambridge Microscan 5 electron microprobe. Operating conditions and estimates of precision have been given by Ernst (1989). Distinct differences in the composition of feldspar, olivine, and augite occur between Units 1 and 2.

Feldspar compositions (Fig. 5A) extend from labradorite through oligoclase and finally to anorthoclase, a pattern reflecting increasing differentiation. Unit 1 feldspars range between $An_{68}Or_0$ and $An_{15}Or_{10}$ [*An*-number $= 100 \times Ca/(Ca+Na+K)$; *Or*-number $= 100 \times K/(Ca+Na+K)$ in molar amounts], whereas Unit 2 feldspars range between $An_{40}Or_5$ and An_0Or_{40}. Most Unit 1 rocks contain only plagioclase, although some that contain andesine and oligoclase also contain orthoclase (An_5Or_{60}). The presence of anorthoclase and sodic plagioclase in Unit 2 rocks suggests that the liquid became fairly evolved during crystallization (Carmichael *et al.*, 1974; Cox *et al.*, 1979). Fe (expressed as FeO_T) ranges between 0·2 and 0·6% at high *An*-number to 0·1–0·3% at low *An*-number. Plagioclase in Unit 1 rocks generally contains <0·1% BaO; in Unit 2 rocks, plagioclase contains up to ~0·5% BaO. Anorthoclase overgrowths on plagioclase contain up to 1·0% BaO.

With increasing magma evolution, the composition of augite changes from En_{73} to En_{38} [$100 \times Mg/(Mg+Fe)$] (Fig. 5B), Al_2O_3 decreases from ~4 to 1%, TiO_2 decreases from ~2 to 0·6%, MnO increases from 0·2 to 0·5%, CaO varies between 21·5 and 20%, Na_2O varies between 0·6 and 0·3%, and SiO_2 varies between 50 and 52%. Unit 1 augites range in composition from En_{75} to En_{55}; those from Unit 2 range from En_{60} to En_{45}. The break between Unit 1 and 2 compositions occurs at an Al_2O_3 content of ~2%, a TiO_2 content of ~1·1% and an MnO content of 0·32%. Based on Ti content, the augite in the GAD typically has a composition intermediate between common augite and titanaugite (Deer *et al.*, 1966).

With increasing magmatic evolution, olivine composition changes from Fo_{68} to Fo_{10} [$100 \times Mg/(Mg+Fe)$] (Fig. 5C), SiO_2 decreases from 37 to 30 wt.%, MnO increases from 0·5 to 1·6 wt.%, and CaO varies between 0·1 and 0·6 wt.%. Most olivines from Unit 1 samples have compositions between Fo_{60} and Fo_{30}; most Unit 2 olivines range between Fo_{35} and Fo_{20}. The break between Unit 1 and 2 compositions occurs at a SiO_2 content of about 33%, and a MnO content of about 1%.

The degree of feldspar zoning (both normal and reversed) is highly variable and commonly large, i.e., up to 30 in terms of *An*-number (Table 2). In contrast, most olivine and augite grains (except for those adjacent to iron–titanium oxides) show only weak zonation, but inter-grain differences in olivine and augite composition are commonly large. That inter-grain variation frequently exceeds within-grain variation (zoning) in olivines and augites suggests only minor re-equilibration by post-crystallization diffusion.

Ilmenites of the GAD have a composition of approximately Ilm_{95} (along the ilmenite–hematite solid solution series), and titanomagnetite lies between Usp_{32} and Usp_{66} (along the ulvöspinel–magnetite solid solution series).

Minor alteration has been noted in samples from the GAD: some olivine is partially replaced by serpentine; augite can be rimmed by amphibole and some plagioclase is partially replaced by a very fine cloud of sericite and epidote. The minor presence of prehnite, chamosite, and pectolite (confirmed by microprobe analyses; Ernst, 1989) indicates minor hydrothermal alteration (Deer *et al.*, 1966, 1978).

WHOLE-ROCK CHEMISTRY

The major elements and Ba, Cr, Zr, Sr, Rb, Y, Nb, Zn, Ni, and V for 187 samples were determined by X-ray fluorescence (XRF) from fused glass discs using a Phillips PW1410/20 AHP machine. One hundred and sixteen samples were analyzed for ferrous iron using the modified cold method of Wilson (Johnson & Maxwell, 1981). The REE, Co, Ta, Sc, Hf, and

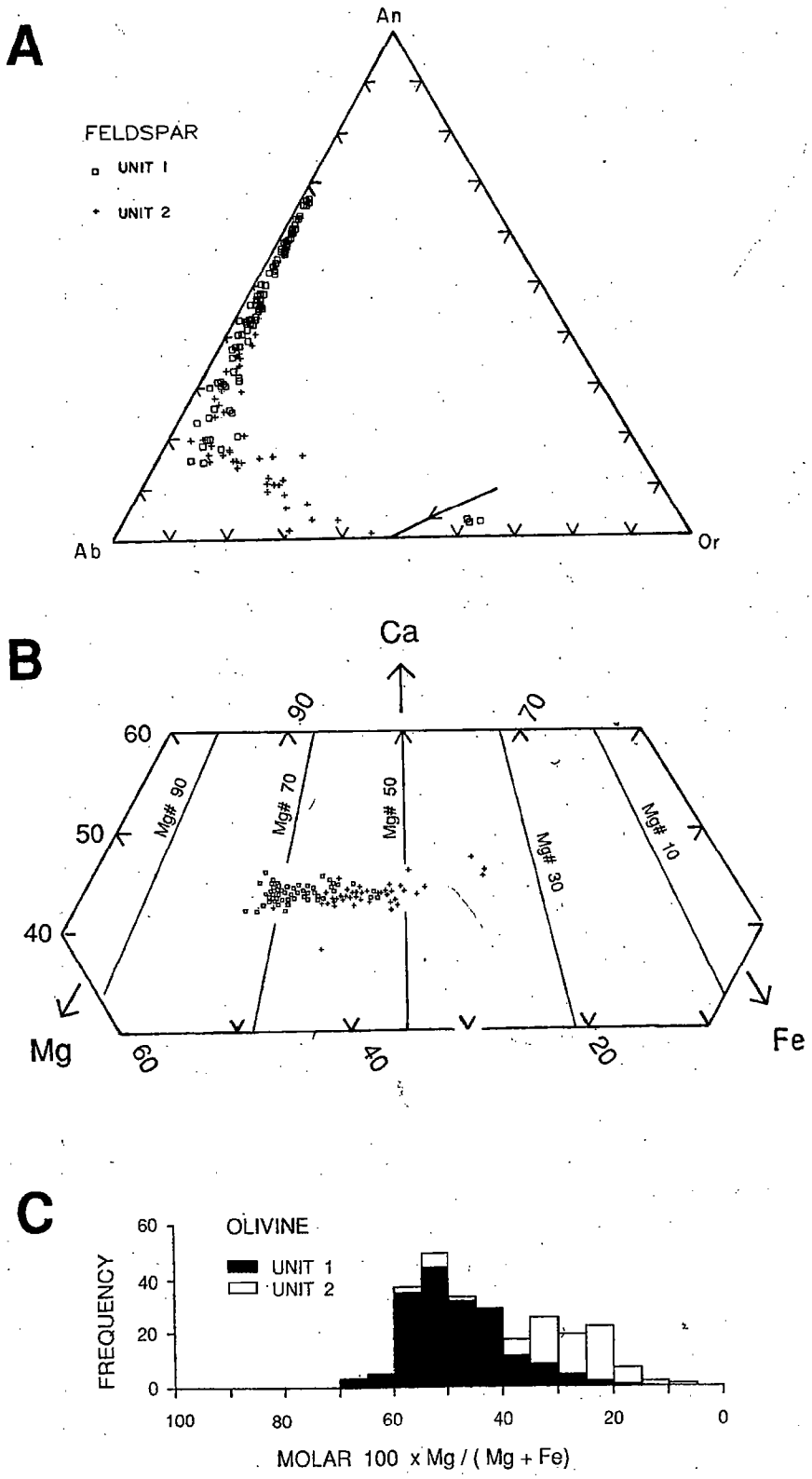

FIG. 5. Mineral chemistry of the GAD. (A) Feldspar chemistry. Arrow marks the boundary curve which describes the composition of the evolving liquid in equilibrium with both orthoclase and plagioclase. (B) Augite compositions plotted on section of pyroxene quadrilateral. (C) Olivine compositions. For (A) and (B) squares and crosses distinguish Unit 1 and Unit 2 rocks respectively. In (B) and (C), Fe is total Fe.

TABLE 2

Compositional variation within and between mineral grains

(A) Variation in *mg*-number [100 × Mg/(Mg+Fe)] in olivines and augites

	Grain 1	*Grain 2*	*Grain 3*	*Grain 4*
		Olivine		
Traverse 2,* Unit 1, 27·1 m from N margin	39 (C)	52 (C)	53 (C)	
	32 (†)	51	50	
	42		51	
	36		49	
	32 (†)		34 (†)	
Traverse 2, Unit 1, 19·1 m from S margin	57 (C)	53 (C)	46 (C)	
	56 (C)	49	47	
	57	50	40	
			43	
Traverse 7,* Unit 1a, 15·0 m from N margin	63 (C)	56 (C)	61 (C)	
	63	56	61	
		57		
		Augite		
Traverse 2, Unit 1, 27·1 m from N margin	63 (C)	68 (C)	69 (C)	
	63	68	69	
	62	67 (†)		
Traverse 7, Unit 1b, 14·2 m from N margin	70 (C)	70 (C)	72 (C)	69 (C)
	70 (C)	71	71	70
	70	70		
	70			

* Dyke widths at traverses 2 and 7 are 88·5 and 209·5 m, respectively.

(C), analysis from core of grain; all other analyses are from the rim (located between ~15 and 50 μm away from grain boundary) or from a position intermediate between core and rim.

(†) rim analysis adjacent to iron–titanium oxide grain.

Th were analyzed using instrumental neutron activation analysis (INAA) at the University of Toronto, following the procedure of Barnes & Gorton (1984). Analytical details have been given by Ernst (1989) and histograms of the data have been given by Ernst *et al.* (1987).

CIPW normative mineral abundances plot on the basalt tetrahedron predominantly in the olivine tholeiite field near the plane of critical undersaturation. The CIPW norm shows strong dependence on the ratio of Fe_2O_3 to FeO. A value of 0·3 was used in the CIPW norm calculations based on the analysis of 116 samples for FeO which gave an average Fe_2O_3:FeO ratio of ~0·3 (±0·1; 2 S.D.). This Fe_2O_3 to FeO ratio is larger than the value assumed by the standard algorithms used to calculate Fe^{2+} and Fe^{3+} from total Fe (Brooks, 1976; Thompson *et al.* 1983). Use of a more 'standard' algorithm for splitting iron shifts the CIPW normative compositions to predominantly weakly silica-undersaturated conditions.

The Nb:Y ratio averages between 0·5 and 0·8 (Table 3 and Ernst, 1989), thus falling on the silica saturated/undersaturated boundary (Winchester & Floyd, 1977), again suggesting a transitional degree of silica saturation. An alkaline affinity is indicated by a plot of total alkalis vs. silica (Ernst *et al.*, 1987). The GAD, therefore, appears to be both weakly silica

TABLE 2 (*Continued*)

(B) Relationship between mineral zonation and adjacent mineral type

Analyzed mineral	*Adjacent mineral*	*Difference between core and rim values** n	$\bar{x}$	*S.D.*
Olivine (*Fo*-number)	Fe–Ti oxide	11	8·6	4·2
	Feldspar	46	2·2	2·9
	Augite	20	0·5	1·7
	Olivine	2	1·5	(range 0·4–2·6)
	Biotite	2	5·5	(range 1·9–9·1)
	Apatite	1	3·3	
Augite (*En*-number)	Fe–Ti oxide	5	1·9	2·0
	Feldspar	24	1·2	3·0
	Olivine	16	3·1	4·8
Feldspar (*An*-number)	Not specified	5	0·6	9·4†
	Not specified	21‡	8·3‡	7·5‡

* *n*, number of 'core minus rim' values. $\bar{x}$, mean value.

† In some cases the core is more calcic than the rim and in other cases the core is more sodic.

‡ For this entry, the range (Max−Min) in *An*-number for individual grains was calculated. *n*, number of grains; $\bar{x}$, average value for the range over the 21 grains.

saturated and also alkaline rich. Other occurrences of alkaline-rich and silica-saturated rocks have been discussed by Miyashiro (1978).

Iron enrichment followed by alkali enrichment is indicated by the GAD data on the AFM diagram (Ernst, 1989). Most Unit 1 data cluster along the iron-enriched portion of the curve, whereas Unit 2 data are distributed along a line heading towards alkali enrichment. The distribution of the data is not consistent with a calc-alkaline trend but is consistent with both tholeiitic and alkaline trends presented by Irvine & Baragar (1971).

It was the bimodal character of the incompatible elements that provided the initial basis for distinguishing the two main units of the GAD (Ernst *et al.*, 1987). In particular, Unit 1 rocks were defined as having <1300 ppm Ba, whereas Unit 2 rocks have Ba contents >1300 ppm. The average composition for each unit is listed in Table 3. In Unit 2 rocks, elements such as Ba, K, Nb, Rb, Y, and Zr are enriched by a factor of about two relative to Unit 1 rocks, whereas Cr, Mg, Ni, and V are more abundant in Unit 1 than Unit 2 rocks. Both *mg*-number and DI (Differentiation Index) data show that Unit 2 represents a higher degree of differentiation than does Unit 1. The differences between average Unit 1 and 2 compositions are statistically significant.

DIFFERENTIATION MECHANISMS

The evolution of the GAD has been modelled using the following assumptions: (1) contamination of the parent magma is relatively small; (2) the entire range of observed chemical compositions from the GAD can be produced by fractional crystallization; and (3) chilled margin compositions give the composition of the parental magma.

Absence of contamination

Crustal contamination in continental magmatism is fairly well documented (e.g., Carlson, 1981) and although such a mechanism might have produced chemical variation in the GAD,

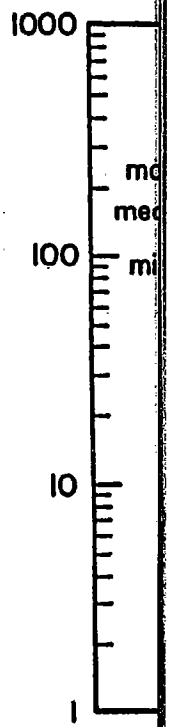

evaluation of the whole-rock chemistry of the GAD suggests contamination is unlikely. Incompatible element spidergrams based on 163 samples from various parts of the GAD have been normalized to the same Y value to remove the effects of fractionation (Fig. 6). The normalized data are tightly grouped for most elements. The wide spread in normalized Sr, Ti, and perhaps P (Fig. 6) is attributable to compatibility in plagioclase, ilmenite, and apatite respectively, and that shown by Rb may be attributed to alteration or contamination of some chilled margin and mini-dyke samples. Despite an unusual pattern (cf. Thompson *et al.*, 1984) of positive and negative anomalies, the normalized data converge to a common spidergram. The spidergrams of possible crustal contaminants, such as those given by Thompson *et al.* (1984), are difficult to match with those shown in Fig. 6. It therefore seems unlikely that the shape and spread of the GAD spidergrams are the result of variable mixing with host rocks. Isotopic work is planned to test further for contamination. In any case, any contaminant must have affected the parental magma only, and does not explain inter-sample variation.

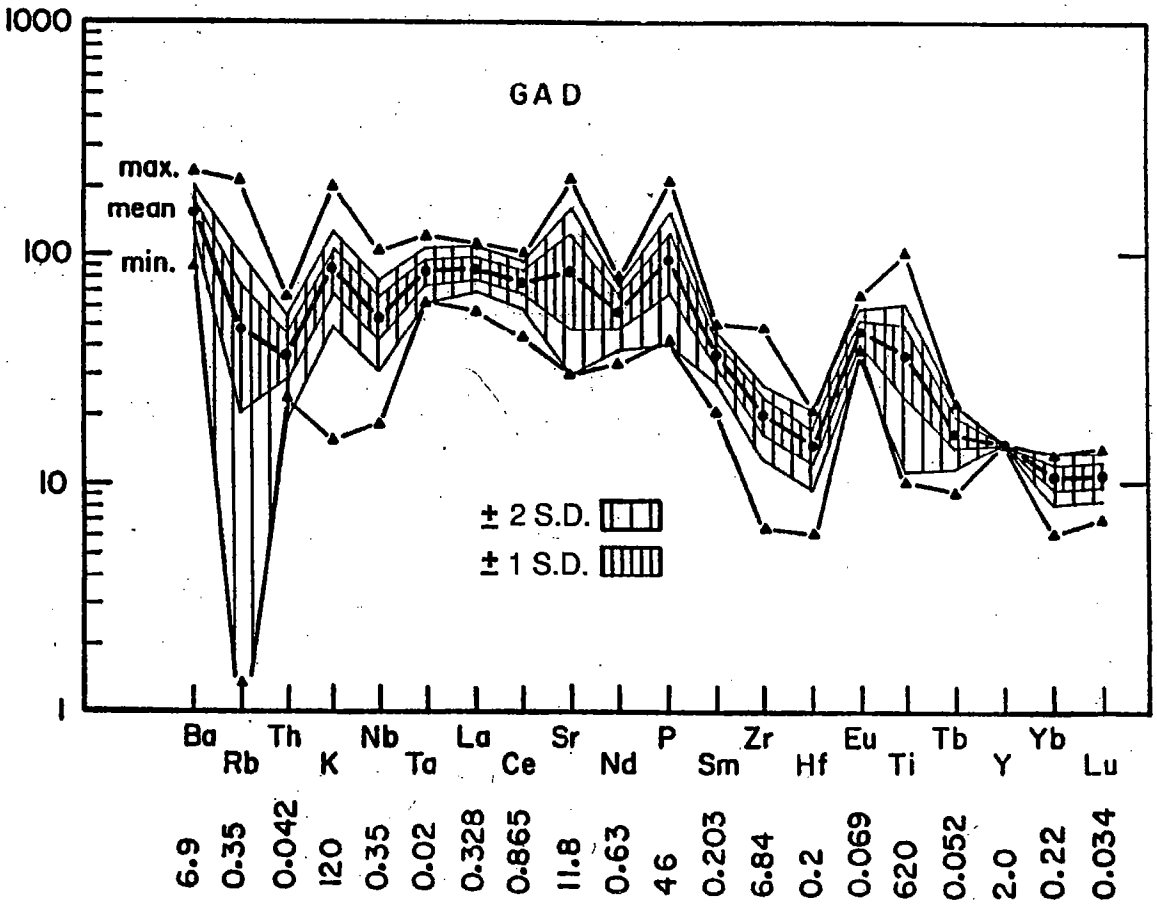

FIG. 6. Doubly normalized spidergrams of GAD data. Data for each element are first divided by the appropriate 'mantle' normalization factor (Thompson *et al.*, 1983; McBirney, 1984, for Eu). Data are further normalized by the ratio 15/Y. This has the effect that all patterns are shifted slightly up or down so that the normalized Y value for each sample equals 15. The mean, 1 S.D. and 2 S.D. envelopes, and maximum and minimum values are calculated from the doubly normalized spidergrams (for all Unit 1 and 2 data combined). The values for Ba, Rb, K, Sr, P, Zr, Ti, and Y are each based on 158 analyses (118 from Unit 1 samples and 40 for Unit 2 samples). The Nb value is based on 125 samples (88 for Unit 1 samples and 37 for Unit 2 samples). Values for each of the remaining elements are based on 50 analyses (45 for Unit 1 samples and 5 for Unit 2 samples).

TABLE 3

Chemical composition of the GAD

	Unit 1 average[1]			*Unit 2 average*[1]			*Chilled margin*[2]				
	n	$\bar{x}$	*S.D.*	n	$\bar{x}$	*S.D.*	*7*[3]	*10*[3]	*14*[3]	*15*[3]	*Average*
SiO_2	121	46·47	1·35	42	48·64	2·95	44·74	45·41	45·81	44·70	45·16
TiO_2	121	3·39	0·79	42	3·19	0·74	3·48	3·22	3·37	3·46	3·38
Al_2O_3	121	17·71	1·60	42	14·64	2·67	16·90	17·01	16·73	16·22	16·71
Fe_2O_{3T}							15·10	14·28	14·47	14·63	14·62
Fe_2O_3	121	2·86	0·69	42	3·63	0·86	—	—	—	—	—
FeO	121	9·70	1·26	42	10·87	3·20	—	—	—	—	—
MgO	121	5·32	1·36	42	2·97	0·86	6·70	6·54	6·33	6·28	6·46
CaO	121	9·15	0·61	42	8·23	0·63	9·14	8·86	8·92	8·77	8·92
Na_2O	121	3·42	0·33	42	4·09	0·58	2·92	3·06	3·31	3·09	3·10
K_2O	121	1·00	0·26	42	1·91	0·23	0·64	0·73	0·92	0·99	0·82
P_2O_5	121	0·81	0·38	42	1·61	0·44	0·63	0·78	0·77	0·83	0·75
MnO	121	0·17	0·02	42	0·22	0·06	0·18	0·18	0·18	0·20	0·19
Zr	121	108	22	42	188	30	81	107	106	113	102
Y	121	24	5	41	41	4	23	24	23	26	24
Nb	121	15	4	42	27	4	13	16	15	14	14
Zn	121	103	24	42	142	27	108	101	112	162	121
Ba	121	835	165	42	1554	142	624	840	817	855	784
Rb	121	13	9	42	26	6	7	7	9	6	7
Sr	121	890	110	42	718	99	878	819	872	794	841
Ni	121	34	23	42	<5	—	60	53	56	47	54

Nb	121	15	4	42	27	4	13	16	15	14	14
Zn	121	103	24	42	142	27	108	101	112	162	121
Ba	121	835	165	42	1554	142	624	840	817	855	784
Rb	121	13	9	42	26	6	7	7	9	6	7
Sr	121	890	110	42	718	99	878	819	872	794	841
Ni	121	34	23	42	<5	—	60	53	56	47	54
Cr	84	61	30	19	15	18	—	67	—	51	59
V	95	243	71	20	136	52	—	225	255	225	235
Co	45	41	8	6	32	12	—	—	50	49	49
Ta	45	1·4	0·3	6	2·3	0·3	—	—	1·4	1·4	1·4
Sc	45	21	4	6	29	9	—	—	22	23	22
Hf	45	2·4	0·5	6	3·9	1·1	—	—	2·3	2·1	2·2
Th	43	1·3	0·4	6	2·5	0·5	—	—	1·1	1·4	1·3
La	45	24	6	6	43	4	—	—	23	22	23
La/Yb	45	13	1	6	12	1	—	—	12	12	12
Eu/Eu*	45	1·5	0·2	6	1·3	0·2	—	—	1·4	1·3	1·4
An-number	121	53	5	42	32	5					
mg-number	121	49	6	42	33	4					
DI	121	35	4	42	46	6					

[1] Major element data were normalized to 100% before being averaged.
[2] Major element data not normalized to 100%.
[3] Traverse numbers.

Total iron (Fe_2O_{3T}) was split into ferric and ferrous forms before computing Unit 1 and 2 averages. Split ratio (Fe_2O_3/FeO) equaled the average value of 0·3 determined on 116 samples.

All oxide-values are in weight percent. All trace elements are in ppm.

An-number is $100 \times An/[An+Ab+Ne(5/3)]$ where An, Ab, and Ne are CIPW normative mineral abundances divided by their molecular weight. *mg*-number = molar $100 \times Mg/(Mg+Fe^{2+})$. DI (Differentiation Index) = Q + Or + Ab + Ne + Ks + Lc (CIPW wt.% normative mineral abundances).

A statistical comparison (*t*-test) of the chemistry of two groups of the freshest near-margin samples was used to evaluate for *in situ* contamination (Ernst, 1989). One group of samples, from traverses 5, 6, 7, 12, and 13, is hosted by potassic granite, whereas the remaining samples are from traverses hosted by volcanic and metamorphic rocks, which are mafic to intermediate in composition. There are no significant differences (at the 95% confidence level) between the chemical composition of the two groups for any elements. However, Rb and Sr in mini-dyke samples and Rb in some visibly altered near-margin samples exhibit large ranges of composition, probably indicating some contamination of these elements.

Very minor, *in situ* contamination of the dyke by the host rock and of the host rock by the dyke may possibly be reflected in compositional profiles across the dyke–host rock contact at two of the traverses (Fig. 7; Ernst, 1989), one where the dyke is bordered by granitoid host rock and the other where it is bordered by mafic–intermediate volcanics. The evidence from both profiles suggests that *in situ* contamination is minimal and at worst affected less than the outer 0·5 m of the dyke. Dyke samples adjacent to mafic/intermediate volcanic wall rock (traverse 10), may have been slightly depleted in Ba, K, Na, Sr, and Zr, whereas adjacent to the granitic wall rock (traverse 7), the dyke appears slightly enriched in Ca, K, Rb, and Si. Some host rocks adjacent to the dyke have undergone minor contact metamorphism; pink granitoid host rocks within ~0·5 m of the contact are 'bleached' white, and mafic–intermediate volcanics within ~2 m of the contact are epidotized.

Evidence for fractional crystallization

Bulk distribution coefficients can be calculated for different elements assuming fractional crystallization (Table 4) (Allègre *et al.*, 1977). Elements are considered in pairs; one element was considered perfectly incompatible and the bulk *D* for the other was calculated assuming crystal fractionation. Ba, Th, and La were considered in turn as being perfectly incompatible. From Table 4 it can be seen that the calculated bulk *D* for all elements was approximately the same regardless of which of these three elements was used. Elements such as Zr, Nb, Y, Ba, Ta, Hf, K, and the REE (except for Eu), behave incompatibly, whereas Ti, P, Zn, and particularly, Sr, V, Ni, Cr, and Co behave compatibly. Those elements shown (in Table 4) to be incompatible are reasonable choices for mafic systems undergoing crystal–liquid fractionation. Zr and Hf are compatible only in zircon and baddeleyite, which are present in trace amounts only. Nb, Ta are weakly compatible only in the accessory phase iron–titanium oxides, Y is found only in apatite which is an accessory phase, and the REE (except for Eu) are hosted in apatite and more weakly in the silicate minerals. Ba and K are compatible in alkali feldspar, but alkali feldspar began crystallizing too late to have been fractionally removed. Ba is slightly compatible in plagioclase. The identification of compatible elements in Table 4 is also sensible. The behaviour of Sr can be attributed to plagioclase fractionation, that of V to titanomagnetites, and that of Ni, Cr, and Co to olivine. The behaviour of Rb may be attributed to contamination of some near-margin and mini-dyke samples. The bulk distribution coefficients calculated using a model of fractional crystallization (Table 4) are consistent with the observed GAD mineralogy, and on this basis, fractional crystallization provides a reasonable explanation for the variation in GAD chemistry. The observed large degree of compositional heterogeneity on a thin-section scale favours fractional rather than equilibrium crystallization.

Chilled margin chemistry

The chilled margin samples have similar chemical composition along a considerable length of the GAD (Table 3). Of the analyses, the sample from traverse 7 is considered the

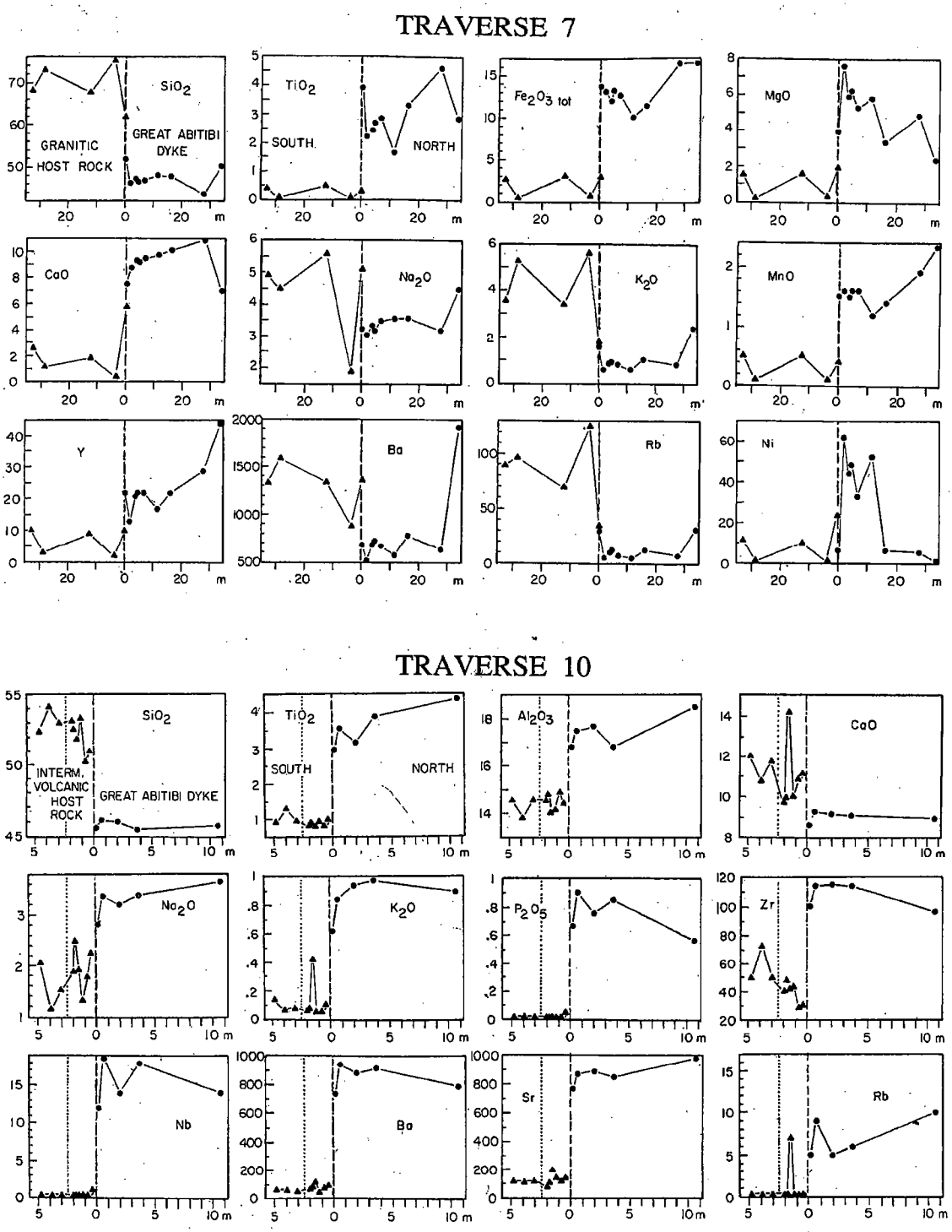

FIG. 7. Evaluation of *in situ* contamination at traverses 7 and 10. Chemical data are plotted along a profile perpendicular to the dyke trend, centered on the dyke–host rock contact. ●, dyke samples; ▲, host rock samples. At traverse 7, the host rock is granite, whereas at traverse 10 the host rock is andesite. The dotted line at the 0 m position marks the contact. The pair of dotted lines on the traverse 10 profiles delimit a zone of contact metamorphosed host rock. For the major elements the analytical uncertainty (±2 S.D.) is no larger than the size of the symbols used for plotting. For minor and trace elements the error ranges up to approximately twice the size of the plot symbol.

TABLE 4

Bulk distribution coefficients calculated from the data-slope on a log(A) vs. log(B) plot; assuming a process of fractional crystallization, the data-slope equals $(D_A-1)/(D_B-1)$, *where* D_A *and* D_B *are the bulk distribution coefficients of elements* A *and* B (D_B *is calculated assuming that* D_A *equals zero and* A *is set equal to Ba, Th, and La in turn*)

	$D_{Ba}=D_A$ $D_A=0$		$D_{Th}=D_A$ $D_A=0$		$D_{La}=D_A$ $D_A=0$	
B	D_B	$S(D_B)$	D_B	$S(D_B)$	D_B	$S(D_B)$
Zr	0·01	0·04	0·13	0·08	0·00	0·09
Hf	0·08	0·08	0·19	0·07	0·08	0·07
Y	0·07	0·04	0·18	0·07	0·06	0·04
Ba	0·00	0·00	0·12	0·07	−0·01	0·07
K	−0·20	0·04	−0·06	0·07	−0·21	0·09
Th	−0·14	0·09	0·00	0·00	−0·15	0·08
La	0·01	0·07	0·13	0·06	0·00	0·00
Ce	−0·01	0·08	0·11	0·06	−0·02	0·02
Nd	−0·13	0·09	0·01	0·08	−0·14	0·05
Sm	−0·07	0·09	0·06	0·08	−0·08	0·03
Yb	−0·01	0·07	0·12	0·07	−0·02	0·03
Lu	0·08	0·07	0·19	0·06	0·07	0·04
Nb	−0·26	0·06	−0·11	0·11	−0·27	0·09
P	−0·58	0·09	−0·39	0·16	−0·59	0·11
Ta	0·18	0·06	0·28	0·05	0·18	0·04
Ti	0·21	0·06	0·30	0·10	0·20	0·11
Zn	0·24	0·05	0·33	0·09	0·23	0·09
Sc	0·34	0·09	0·42	0·08	0·33	0·08
Eu	0·23	0·06	0·32	0·06	0·22	0·04
Rb	−1·10	0·13	−0·85	0·21	−1·12	0·26
Sr	1·49	0·03	1·43	0·05	1·50	0·05
V	2·33	0·11	2·17	0·13	2·34	0·17
Ni	3·42	0·19	3·13	0·27	3·44	0·32
Cr	3·47	0·20	3·17	0·29	3·49	0·31
Co	1·78	0·08	1·69	0·07	1·79	0·09

The best-fitting slope was calculated using the 'reduced major axis' method discussed by York (1966). $S(D_B)$ is the 1 S.D. calculated from analytical uncertainties in element abundances using the error propagation equations given by Kretz (1985).

Negative values for D_B are meaningless and must be due to (1) $D_A > D_B$, in violation of an assumption of the method, (2) analytical uncertainty, or (3) in the case of Rb, some contamination by host rock.

most primitive, and therefore, is used as the best estimate of the chemical composition of the parent magma. The chilled margin sample from traverse 7 has the lowest abundance of incompatible elements (e.g. Zr, Ba, and K) and has the highest MgO and Ni contents of any of the chilled margin samples. Although plagioclase phenocrysts are present in all chilled margin samples, arguments discussed below show that these feldspars grew *in situ*.

MODELLING OF COMPOSITIONS USING PEARCE ELEMENT RATIO ANALYSIS

Compositional variation in the Great Abitibi Dyke is attributed to liquid–crystal fractionation. The mineral assemblage involved in this process can be identified using Pearce element ratio (PER) diagrams.

Pearce element ratio diagrams were originally developed by Tom Pearce in 1968 to defeat the closure problem which limits the effectiveness of Harker diagrams in graphical modelling of petrogenetic trends. A brief explanation of the approach follows. More detailed explanations have been given by Russell & Stanley (1990*a*) and in references therein, as well by Pearce (1968), Ernst *et al.* (1988), Nicholls & Stout (1988); Russell & Nicholls (1988), Stanley & Russell (1989) and Russell & Stanley (1990*b*). The possibility of spurious correlations on PER diagrams, as raised by Rollinson & Roberts (1986), has been fully addressed in the more recent publications above.

In geology, chemical compositions are ordinarily presented as intensive variables (e.g., fractional abundances, wt.% or ppm). However, for a suite of cogenetic samples all having crystallized from the same parental magma, we can envision underlying extensive variables (absolute amounts, e.g., mass, volume or molar units), which relate to a common parental magma (Russell & Stanley, 1990*b*). Fractional abundances can be related to these absolute abundances as follows:

$$A+B+\ldots+Z=1\ (100\%)$$

where A, B, and Z equal fractional abundances.

$$A=A/S$$

$$B=B/S$$

$$Z=Z/S$$

where $\boldsymbol{A}$, $\boldsymbol{B}$, $\boldsymbol{Z}$, and $\boldsymbol{S}$ are extensive variables and $\boldsymbol{S}$ represents the size of the system, i.e., the amount of magma. Therefore a Harker diagram (a plot of A vs. B) is actually a ratio plot of $\boldsymbol{A/S}$ vs. $\boldsymbol{B/S}$. In general, the size, $\boldsymbol{S}$, of the magma chamber (i.e., the amount of magma remaining) will be changing as the magma crystallizes, and therefore data distributions on a Harker diagram will be controlled not only by $\boldsymbol{A}$ and $\boldsymbol{B}$, but by $\boldsymbol{S}$ as well. But, of course, variation in $\boldsymbol{S}$ will be controlled by the variation in all the elements. Hence trends on Harker diagrams cannot be directly related to the process controlling variation in $\boldsymbol{A}$ and $\boldsymbol{B}$.

Pearce element ratio diagrams, by contrast, are plots of A/Z vs. B/Z, where Z is a conserved element (that is, an element which is neither added to nor subtracted from the system). Let us consider the system to be a magma chamber, where Z is an incompatible element. As the magma crystallizes, the incompatible elements are conserved, in the sense that they are always partitioned into the remaining liquid and are not removed from the system as crystallizing minerals. (For a sample suite related by variable degrees of contamination, an immobile element would be an appropriate choice for the conserved variable, Z.) The axes of PER diagrams expressed as intensive variables, A/Z vs. B/Z, can be given in extensive form as $(\boldsymbol{A/S})/(\boldsymbol{Z/S})$ vs. $(\boldsymbol{B/S})/(\boldsymbol{Z/S})$, which reduces to $\boldsymbol{A/Z}$ vs. $\boldsymbol{B/Z}$. When Z is conserved, then $\boldsymbol{Z}$ is constant and the diagram becomes $\boldsymbol{A/Z_0}$ vs. $\boldsymbol{B/Z_0}$. Thus on a PER diagram, unlike a Harker diagram, the data distribution is due to only the relative variation in $\boldsymbol{A}$ and $\boldsymbol{B}$. Stated another way, on a PER diagram the data from a cogenetic suite of samples are distributed along a trend with a slope equal to the bulk $\boldsymbol{A:B}$ ratio in the minerals lost or gained from the parental magma.

In the case of the GAD, intersample variation is attributed to fractional crystallization and therefore the conserved denominator variable should be an incompatible element. Calculations by Ernst *et al.* (1988) and Ernst [Chapter 11 in Russell & Stanley (1990*a*)] show that even if an element is slightly compatible such that its bulk distribution coefficient reaches 0·1, the error produced on PER diagrams is insignificant. With this criterion, any of the incompatible elements identified in Table 4 could be used for the denominator element

in the PER analysis. Each analysis will be done using more than one choice of denominator element, to preclude biased trends attributable to the use of any one element.

Simple numerator-type Pearce element ratio (PER) diagrams

Simple numerator-type PER diagrams (A/Z vs. B/Z) were used to determine the bulk composition of the mineral assemblage which was lost (fractionated out of the system) or concentrated as cumulates during fractionation of the parental magma (Fig. 8 and Table 5). Ba and La were each used as the constant denominator variable, Z; use of either leads to the same conclusions. La was analyzed for a representative subset (one-third) of the samples and Ba was analyzed for all samples. For the PER diagrams in Fig. 8, the ordinate (y-axis) numerator is Si and the abscissa (x-axis) numerator is cycled through all the major elements. Si was chosen for comparison with all other elements because it is the most abundant cation, and because it is a component of most of the major mineral phases which could conceivably be fractionated from the GAD magma.

TABLE 5

Average chemical composition of the mineral assemblage responsible for inter-sample variation, as determined using Pearce element ratios

A	A′* (*wt.* %)	S(A′)†	A′ (*wt.* %)	S(A′)
		Units 1 *and* 2		
SiO_2	44·42	0·41	42·08	0·32
TiO_2	3·60	0·26	3·64	0·20
Al_2O_3	20·65	0·31	20·20	0·26
FeO	8·82	0·43	9·66	0·37
Fe_2O_3	2·66	0·15	3·13	0·20
MgO	7·69	0·33	9·12	0·24
CaO	9·12	0·23	9·50	0·17
Na_2O	2·89	0·09	2·52	0·06
K_2O	0·56	0·06	−0·56	0·04
P_2O_5	−0·63‡	0·08	−1·09	0·08
MnO	0·16	0·01	0·15	0·01
Total	100·00		100·00	
Fe_2O_{3T}	12·34	0·71	13·03	0·61
		Z§ = La		Z = Ba
		n§ = 51		n = 163
		Unit 1		
SiO_2	44·61	0·43	40·83	0·48
TiO_2	3·68	0·30	3·86	0·32
Al_2O_3	20·28	0·33	19·33	0·41
FeO	9·07	0·43	10·25	0·50
Fe_2O_3	2·67	0·15	4·02	0·32
MgO	7·87	0·36	10·22	0·38
CaO	8·91	0·24	8·92	0·26
Na_2O	2·76	0·10	2·38	0·09
K_2O	0·56	0·06	−0·77	0·07
P_2O_5	−0·63	0·08	−1·45	0·13
MnO	0·16	0·01	0·19	0·01
Total	100·00		100·00	
Fe_2O_{3T}	12·69	0·71	13·84	0·84
		Z = La		Z = Ba
		n = 45		n = 121

TABLE 5 (*Continued*)

A	A′* (wt. %)	S(A′)†	A′ (wt. %)	S(A′)
		Unit 2		
SiO_2	56·87	2·07	47·70	1·62
TiO_2	−4·23	1·23	−10·02	1·61
Al_2O_3	30·63	2·16	30·75	1·66
FeO	−16·93	4·72	−41·29	6·60
Fe_2O_3	−5·82	1·63	−11·28	1·83
MgO	−6·53	1·65	−11·52	1·86
CaO	2·97	0·66	12·60	1·50
Na_2O	6·98	0·78	6·57	0·60
K_2O	2·54	0·30	2·39	0·26
P_2O_5	−2·96	0·66	−5·75	0·93
MnO	−0·34	0·10	−0·73	0·12
Total	100·00		100·00	
Fe_2O_{3T}	−24·64	6·87	−54·32	8·69
	Z=La		Z=Ba	
	n=6		n=42	

* Compositions determined from Pearce element ratio (PER) diagrams of the form Si/Z vs. A/Z, where Z (the conserved element) equals either La or Ba, Si is silicon, and A is cycled in turn through all the other major elements (see Fig. 8). From each plot of Si/Z vs. A/Z, the best-fitting slope was determined using the 'reduced major axis' method (York, 1966). This slope equals $\boldsymbol{A/Si}$. Bold italic variables are in absolute units (e.g., moles, grams). Non-bold variables are in fractional units (e.g., wt. %). The relationship between absolute and fractional abundances is $\boldsymbol{A/S}=A$, where $\boldsymbol{S}$ refers to the absolute size of the system (e.g., Russell & Stanley, 1990*b*). For each element, $A'=100\times(\boldsymbol{A/Si})/\boldsymbol{SUM}$, where $\boldsymbol{SUM}$ can be defined as follows:
(For Unit 1 and combined Unit 1 plus Unit 2 data)
$\boldsymbol{SUM=Si/Si+Ti/Si+Al/Si+Fe^{2+}/Si+Fe^{3+}/Si+Mg/Si+Ca/Si+Na/Si+Mn/Si.}$
(For Unit 2 data)
$\boldsymbol{SUM=Si/Si+Al/Si+Ca/Si+Na/Si+K/Si.}$
† $S(A')$ is the standard deviation of A' calculated from analytical uncertainty using error propagation equations (e.g., Kretz, 1985).
‡ Negative values for A' result from variation opposite to that of Si′.
§ Both La and Ba were used as the conserved denominator element, Z.

The Si content in Unit 1 rocks correlates positively with that of all other elements except for K and P. The most highly correlated trends in Fig. 8 are those in which the abscissa numerator is Al, Mg, Ca, and Na. This requires fractionation of minerals rich in Si, Al, Mg, Ca and Na. In Unit 2 rocks (Table 5) the elements Al, Ca, Na, and K, hosted in feldspar, all show a slight positive correlation with Si. Fe, Mg, and Mn (hosted in mafic silicates) as well as P (hosted in apatite) exhibit a weak negative correlation with Si.

In those plots (see Fig. 8 and Table 5) where Ti, Fe^{2+}, Fe^{3+}, Mn, and P are the abscissa numerator variables, the slope defined by the Unit 2 data differs from that defined by the bulk of the Unit 1 data. This suggests that the minerals containing Ti, Fe, Mn, and P fractionated in different proportions in Unit 1 compared with Unit 2.

Multi-element numerator-type Pearce element ratio (PER) diagrams

The more complicated numerators used in Fig. 9 are designed to test for fractionation of specific minerals (Ernst *et al.*, 1988; Stanley & Russell, 1989). Best-fit slopes were calculated

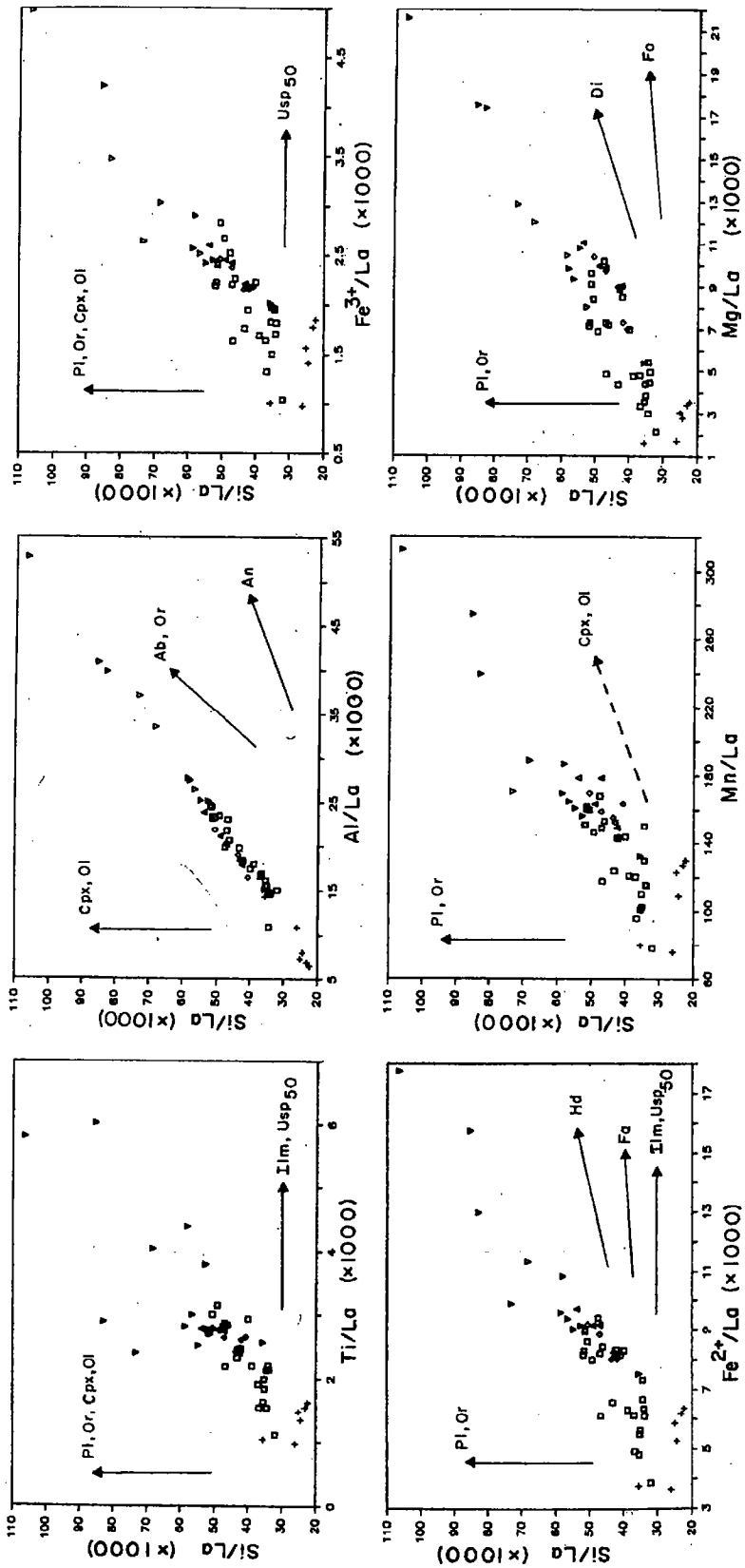
Si/La (x1000)
Ti/La (x1000)
Pl, Or, Cpx, Ol
Ilm, Usp50
Al/La (x1000)
Cpx, Ol
Ab, Or
An
Mn/La
Pl, Or
Cpx, Ol
Fe2+/La (x1000)
Hd
Fa
Ilm, Usp50
Ab, Or, Ol
Mg/La (x1000)
Di
Fo
An, Or, Cpx, Ol
Fe3+/La (x1000)
Usp50
An, Ab, Cpx, Ol

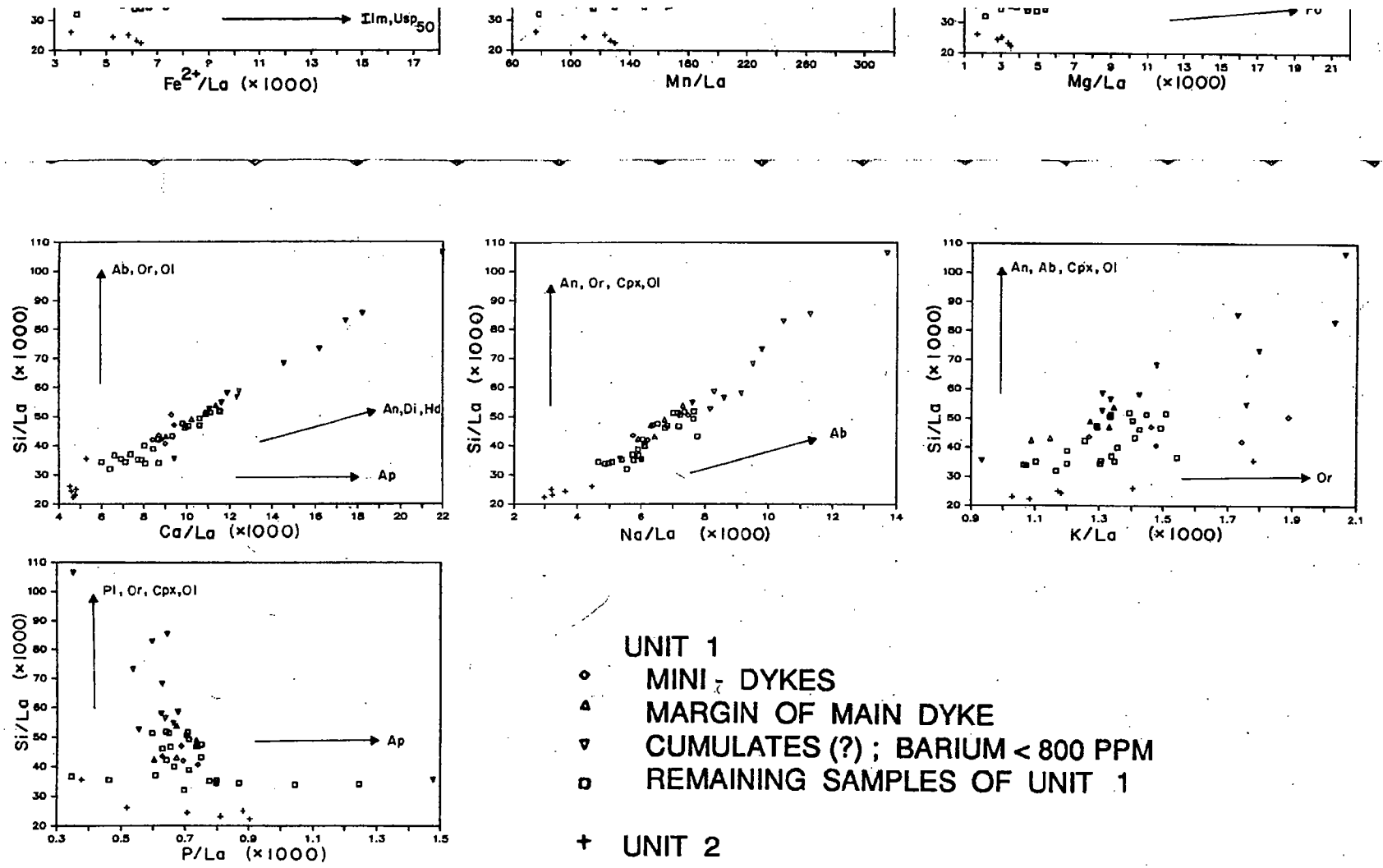

FIG. 8. Pearce element ratio diagrams of major element data using La as the denominator variable. Arrows are reference mineral vectors. Molar abundances were used in calculating ratios. Quantitative analysis of the data is given in Table 5. The 2 S.D. analytical error is no more than approximately three times the size of the plot symbol; it is worst for the plots with minor element numerators.

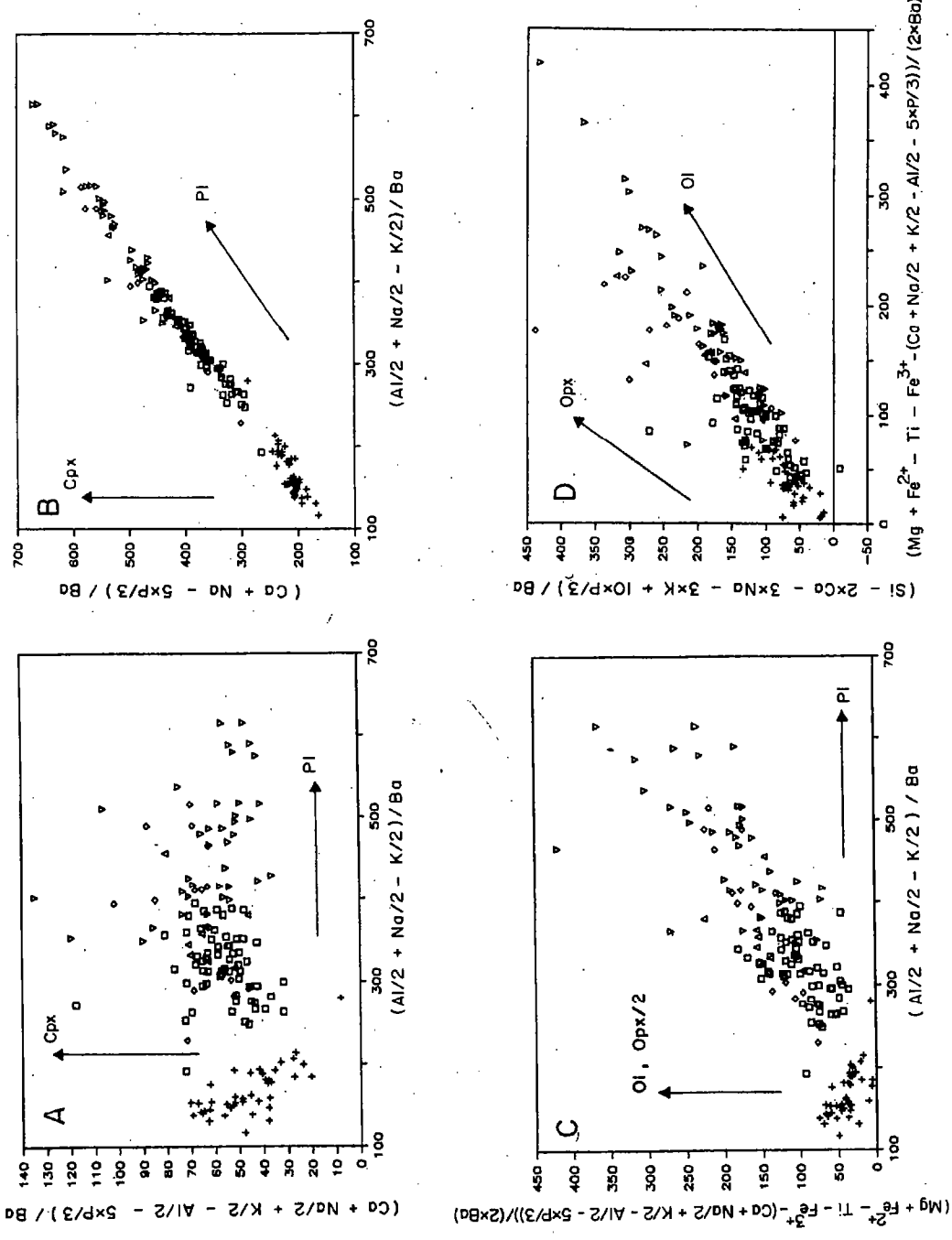
A
Cpx
Pl
(Ca + Na/2 + K/2 - Al/2 - 5xP/3) / Ba
(Al/2 + Na/2 - K/2) / Ba
B
Cpx
Pl
(Ca + Na - 5xP/3) / Ba
(Al/2 + Na/2 - K/2) / Ba
C
Ol, Opx/2
Pl
(Mg + Fe2+ - Ti - Fe3+ -(Ca + Na/2 + K/2 - Al/2 - 5xP/3))/(2xBa)
(Al/2 + Na/2 - K/2) / Ba
D
Opx
Ol
(Si - 2xCa - 3xNa - 3xK + 10xP/3) / Ba
(Mg + Fe2+ - Ti - Fe3+ -(Ca + Na/2 + K/2 - Al/2 - 5xP/3))/(2xBa)
E
Ilm
F
Ap
G

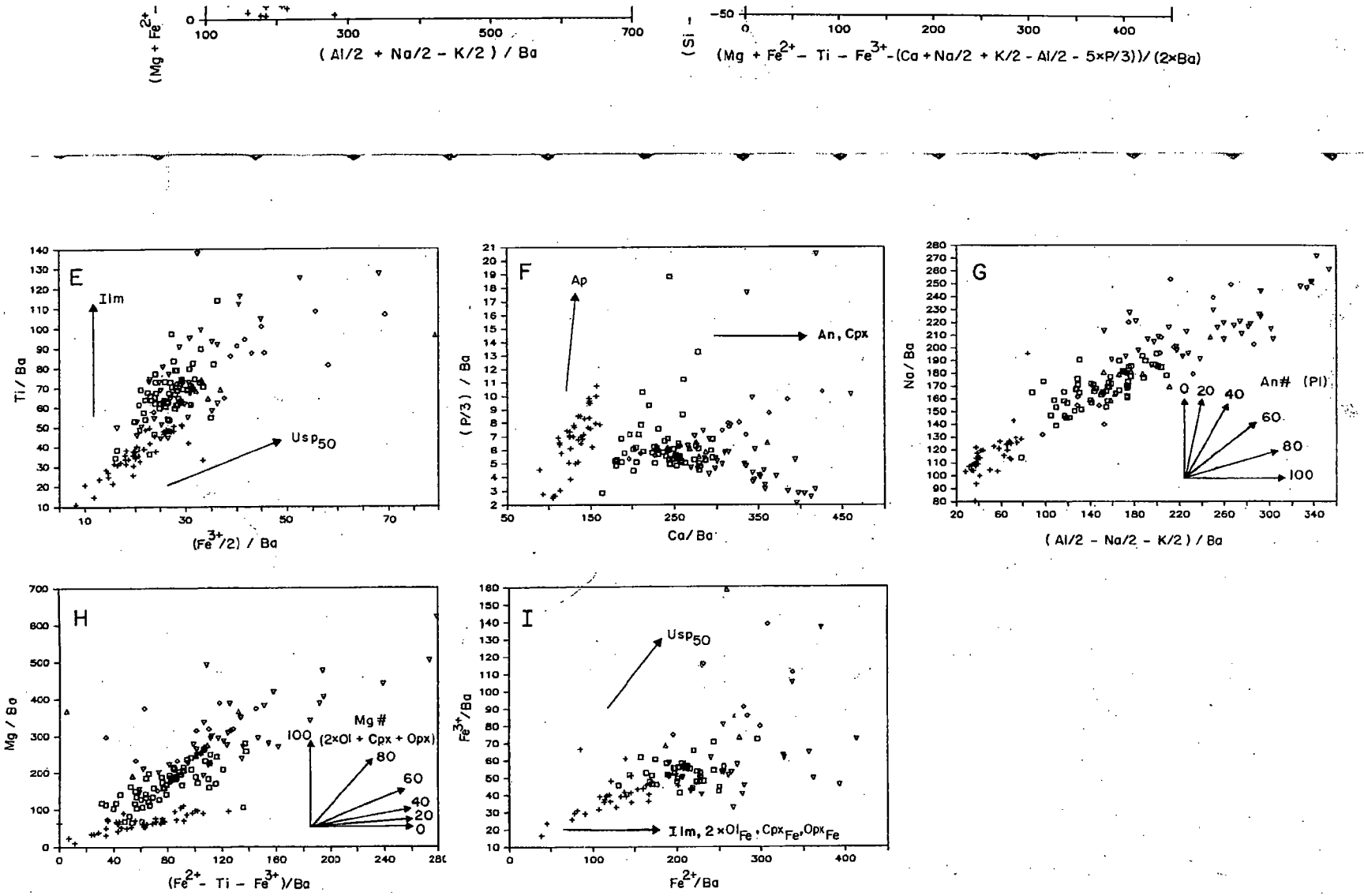

FIG. 9. Pearce ratio diagram using complex numerators designed to test for fractionation of particular mineral phases and to determine the proportions of these phases in the fractionate. Arrows are reference mineral vectors. In (H) the '2 × Ol' written adjacent to the mineral vectors means that on the basis of stoichiometry, olivine (Ol) is twice as effective in controlling the data-slope as is clinopyroxene (Cpx) or orthopyroxene (Opx). Data symbols are the same as in Fig. 8. Molar abundances were used. Quantitative analysis of the data is given in Table 6. The 2 S.D. analytical error is no more than approximately three times the size of the plot symbol.

using both Ba and La as the conserved denominator element (Fig. 9; Table 6). The numerators are designed to discriminate between minerals having ideal stoichiometric compositions and should adequately model the behaviour of those minerals responsible for fractionation in the GAD. For example, the numerator variables in Figs. 9A and 9B are designed for clinopyroxene of the diopside–hedenbergite solid solution series, but these numerators should also adequately reflect the behaviour of augite.

The relative roles of plagioclase and augite (cpx) fractionation can be assessed from Figs. 9A and 9B. In both diagrams, the data from samples of Unit 1 parallel the plagioclase mineral vector and there is only slight variation parallel to the augite (cpx) mineral vector. In Fig. 9A, the variation along the plagioclase vector is ~500 units whereas that along the augite (cpx) vector is about 50 units (note the unequal *x*- and *y*-axis scales). This data distribution demonstrates that the magnitude of plagioclase fractionation exceeds that of augite. Data from Unit 2 have a slope (Table 6) indicating opposite behaviour of plagioclase and augite. According to Fig. 9, as augite was being removed from the melt, plagioclase was being concentrated (as cumulates) in the same melt volume. The inverse interpretation is also allowed by the data—as plagioclase was removed, augite was being concentrated.

The relative contributions of plagioclase, olivine, and orthopyroxene fractionation can be assessed from Figs. 9C and 9D. In Fig. 9D, data from both Unit 1 and 2 rocks parallel the olivine vector more closely than the orthopyroxene vector, indicating fractionation of olivine but not of orthopyroxene. This compositional evidence is consistent with the virtual absence of orthopyroxene as a modal phase in the GAD. Thus in Fig. 9C the orthopyroxene vector can be ignored and the data trend can be entirely attributed to plagioclase and olivine

TABLE 6

Proportions of minerals removed and added during fractionation, determined using Pearce element ratios with multi-element numerators

A	A'* (*mol %*)	S(A')†	A' (*mol %*)	S(A')
	Units 1 and 2			
Plagioclase	59·54	1·23	51·78	0·91
Augite	5·60	0·66	7·40	0·58
Olivine	27·57	1·93	31·43	1·49
Ilmenite	5·68	0·62	6·80	0·86
Apatite	−0·67‡	2·08	−1·03	1·50
Titanomagnetite	1·61	0·19	2·58	0·32
K-Feldspar	2·80	0·29	−2·54	0·20
An-number	62·23	5·77	66·36	5·72
mg-number	78·23	1·50	72·00	1·91
	Z§ = La		Z = Ba	
	n§ = 51		n = 163	
	Unit 1			
Plagioclase	57·91	1·35	45·96	1·22
Augite	5·73	0·74	8·50	0·81
Olivine	28·67	2·20	34·93	2·26
Ilmenite	5·95	0·73	6·87	1·37
Apatite	−0·69	2·26	1·33	2·11
Titanomagnetite	1·74	0·22	3·74	0·62
K-Feldspar	2·95	0·31	−3·26	0·31
An-number	62·89	6·61	67·20	9·43
mg-number	77·32	1·61	69·50	2·54
	Z = La		Z = Ba	
	n = 45		n = 121	

TABLE 6 (*Continued*)

A	A'* (*mol %*)	S(A')†	A' (*mol %*)	S(A')
		Unit 2		
Plagioclase	87·64	0·75	88·18	1·05
Augite	−16·91	3·93	−43·21	4·57
Olivine	−22·79	2·81	−53·88	6·44
Ilmenite	−2·57	1·09	−11·80	6·61
Apatite	−9·57	6·07	5·19	10·05
Titanomagnetite	−2·87	0·71	−7·55	3·38
K-Feldspar	12·36	0·86	11·82	1·20
An-number	41·84	4·89	48·69	10·82
mg-number	59·27	4·26	42·82	13·48
		Z = La		Z = Ba
		n = 6		n = 42

* Compositions determined from Pearce element ratio diagrams of the form A/Z vs. B/Z, where Z (the conserved element) equals either La or Ba, and A and B are linear combinations of major elements designed to represent specific minerals [Fig. 9 and Ernst *et al.* (1988)]. The best-fit slope through the data equals A/B, where A and B are the absolute abundances of A and B. Using the variables plotted in Fig. 9, best-fitting slopes can be directly determined for Cpx/Pl, Ol/Pl, Ilm/Mt, Mt/Fe^{2+}, Mg/Fe^{2+}, Ap/An, and Ab/An. (Titanomagnetite, Mt, is modelled with a composition of Usp_{50}.) Other relationships can be calculated from these as follows:

$Ilm/Pl \sim [Ilm/Mt] \times [Mt/Fe^{2+}] \times [1/\{1+Mg/Fe^{2+}\}] \times [\{2\} \times \{Ol/Pl\} + Cpx/Pl]$

$Ap/Pl = [Ap/An] \times [1/\{1+Ab/An\}] \sim [Ap/\{An+5Ap\}] \times [1/\{1+Ab/An]$

$Mt/Pl \sim [Mt/Fe^{2+}] \times [1/\{1+Mg/Fe^{2+}\}] \times [\{2\} \times \{Ol/Pl\} + Cpx/Pl]$

$Kfs/Pl = [K]/[Al/2+Na/2-K/2]$

$An\text{-number} = 100 \times [1/\{1+Ab/An\}]$

$mg\text{-number} = 100 \times [1-\{1/(1+Mg/Fe)\}]$.

For this analysis it is assumed that the Mg/Fe ratio of olivine and augite are the same. For each mineral, $A' = 100 \times (A/Pl)/SUM$, where SUM can be defined as follows:

(For Unit 1 and combined Unit 1 and 2 data)

$SUM = Pl/Pl + Cpx/Pl + Ol/Pl + Mt/Pl + Ilm/Pl$

(For Unit 2 data)

$SUM = Pl/Pl + K/Pl$.

† $S(A')$ is the standard deviation of A' calculated from analytical uncertainty using error propagation equations (e.g., Kretz, 1985).

‡ Negative values for A' result from inverse variation with Si.

§ Both La and Ba were used as the conserved denominator element, Z.

fractionation. Unit 1 data follow a trend intermediate between the olivine and plagioclase reference vectors, indicating fractionation of both phases. Calculations of the relative contributions of olivine and plagioclase fractionation (Table 6), show that nearly twice as much plagioclase as olivine was fractionated from the original parent magma. Data from Unit 2 samples follow a negative slope, suggesting plagioclase loss and olivine accumulation (or vice versa—olivine loss and plagioclase accumulation).

Figures 9A–D show plagioclase behaving in a contrary manner to both olivine and augite in Unit 2 rocks. As plagioclase is less dense than olivine and augite, a possible explanation (further elaborated below) may be density-controlled segregation.

Figures 9A and 9B show augite fractionation had little control on the composition of Unit 1 rocks. Consequently, the augite mineral vector is ignored and (noting the unequal x- and y-axis scales) Figure 9F shows that the variation in both Units 1 and 2 is controlled to a much greater extent by plagioclase fractionation than by that of apatite.

The role of iron–titanium oxides is assessed in Figs. 9E and 9I. In designing appropriate complex numerators a composition of Usp_{50} was assigned to the titanomagnetites, and

ilmenite was assumed to be pure ilmenite, Ilm_{100}, similar to the analyzed compositions of titanomagnetite and ilmenite in the GAD rocks. The data in Figs. 9E and 9I define a trend with a slope between the slopes of the ilmenite and titanomagnetite (Usp_{50}) reference vectors, indicating that both ilmenite and titanomagnetite were fractionated from the parental liquid in approximately sub-equal proportions.

Normalized Pearce element ratios (PERs)

Chemical compositions of different cogenetic samples are more simply related when converted from fractional to absolute amounts (i.e., from intensive to extensive variables). This is achieved by dividing analyses by the composition of a conserved element and thereby producing a Pearce element ratio (PER). Subtraction of PERs is meaningful. Let us consider fractionating element A, conserved element Z and the size of the system, S at two different states, '0' and 'i':

$$\Delta\text{PER} = A_i/Z_i - A_0/Z_0 = [A_i/S_i]/[Z_i/S_i] - [A_0/S_0]/[Z_0/S_0] = [A_i - A_0]/Z_0$$

provided Z is conserved.

Differences between PERs are more meaningful than differences between wt.% abundances.

$$\Delta(\text{fractional}) = A_i - A_0 = A_i/S_i - A_0/S_0.$$

It is also useful to scale PERs to a convenient reference value, such as the composition of the parental magma, e.g., at state '0'.

$$\Delta\text{PER}_N = [Z_0][A_i/Z_i - A_0/Z_0] = A_i/S_0 - A_0 = [A_i - A_0]/S_0$$

provided Z is conserved.

Pearce element ratios provide a purely chemical definition of cumulates and fractionates. Samples with a PER larger than that of the parent have been enriched in a mineral phase and therefore are by definition, cumulates. Similarly, samples with a PER smaller than that of the parent have lost material through fractionation and are therefore fractionates. PER_N from rocks thoughout the GAD are compared below.

In Fig. 10A CIPW normative abundances are plotted against across-dyke position of the dyke at traverse 7. In Figs. 10B and 11, CIPW normative data are transformed into normalized Pearce element ratios (NPERs). Various choices of incompatible elements, Ba, Zr, Y, and K (Table 4) were tested. All gave essentially the same normalized PER values but this paper displays only the results using Ba (Fig. 10) and a multi-element denominator consisting of Ba, Zr, Y, and K (Fig. 11).

The normalized PER for the parental magma (circled in Fig. 10) equals $NPER_{plag} = 57\%$. A Unit 2 sample in Fig. 10 with $NPER_{plag} = 15\%$ can be derived from the parental magma by fractionation of 40% (~57–15%) plagioclase, corresponding to about 3/4 (40%/57%) of the potentially available plagioclase in the parent. Similar calculations, using the normalized PERs for each CIPW mineral phase, allow an estimate to be made of the amount of any mineral lost from the parental magma to produce any sample of Unit 1 or 2. Figure 10 shows that rocks of Unit 2 (at traverse 7) could have been derived by removal of about 40% plagioclase, 13% olivine, and 5% ilmenite from the parental magma. Formation of Unit 2 magma from the parental magma requires essentially no loss of alkali feldspar (CIPW orthoclase), augite (CIPW diopside), titanomagnetite (CIPW magnetite), or apatite.

The irregular pattern in Unit 1 suggests that the magma was heterogeneous and was probably emplaced in discrete pulses, consistent with field evidence for multiple pulses of

Unit 1a and 1b (Fig. 4). The large spikes inwards from each margin on most plots in Fig. 10B are indicative of cumulates. The amount of accumulation is given by subtraction of normalized PERs from that of the parental magma (circled). These spikes indicate a 10% excess (over the amount in the parental magma) of plagioclase, 6% of augite, 7% of olivine, and 3% of ilmenite, and also a small excess of titanomagnetite and apatite. The cumulate locations differ between plots. Plagioclase and olivine cumulates are located near the boundary between Units 1a and 1b, whereas augite, ilmenite, and apatite (Ernst, 1989) cumulates are located near the boundary between Units 1 and 2.

Compositional asymmetry across Unit 2 is suggested at traverse 7. Normative plagioclase and orthoclase increase towards the south side whereas olivine, diopside (representing

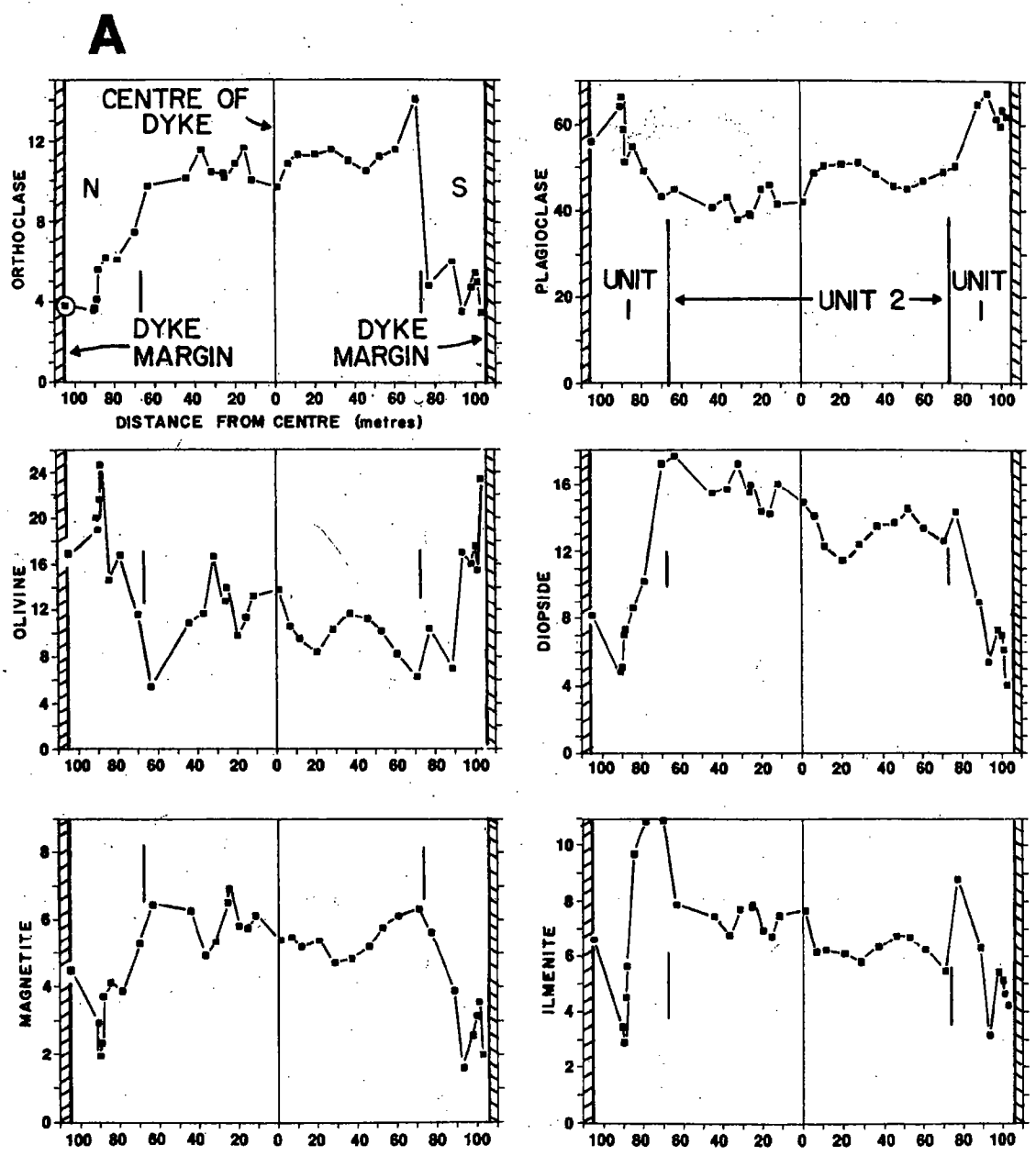

FIG. 10A

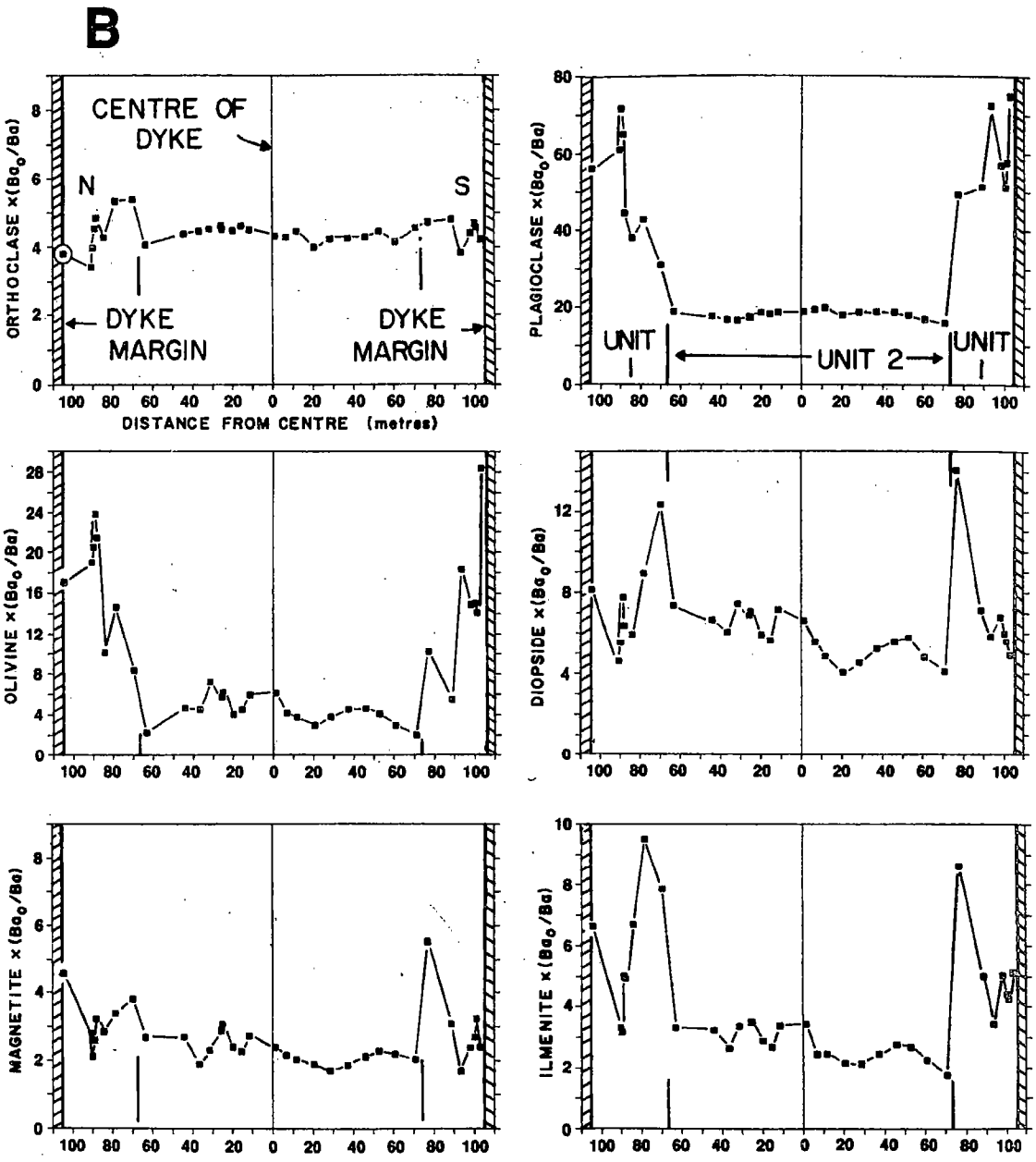

FIG. 10. A comparison of CIPW normative abundances at traverse 7 with the same data converted into PERs. (A) CIPW normative abundance (wt. %) vs. position across the dyke. (B) PERs of CIPW normative abundances. CIPW abundances were normalized by Ba_0/Ba, where Ba is considered a conserved element and Ba_0 is from the chilled margin sample (circled data point) considered to represent the parental composition. Short vertical solid lines locate the boundary between Units 1 and 2.

augite), ilmenite, and perhaps magnetite (representing titanomagnetite) increase towards the north side. The average *Fo*-number of olivine increases from Fo_{18} to Fo_{24}, across Unit 2 from south to north. The asymmetry observed in Unit 2 rocks is also possibly present in rocks of Unit 1b [Fig. 10 and Ernst (1989)].

Such a distribution can be explained by density-controlled segregation of crystals in a melt within a non-vertical dyke-conduit (Komar, 1972; Platten & Watterson, 1987; Cadman *et al.*, 1990). At traverse 7, the dyke dips 70–80 °S (Ernst, 1989) and less dense phases could

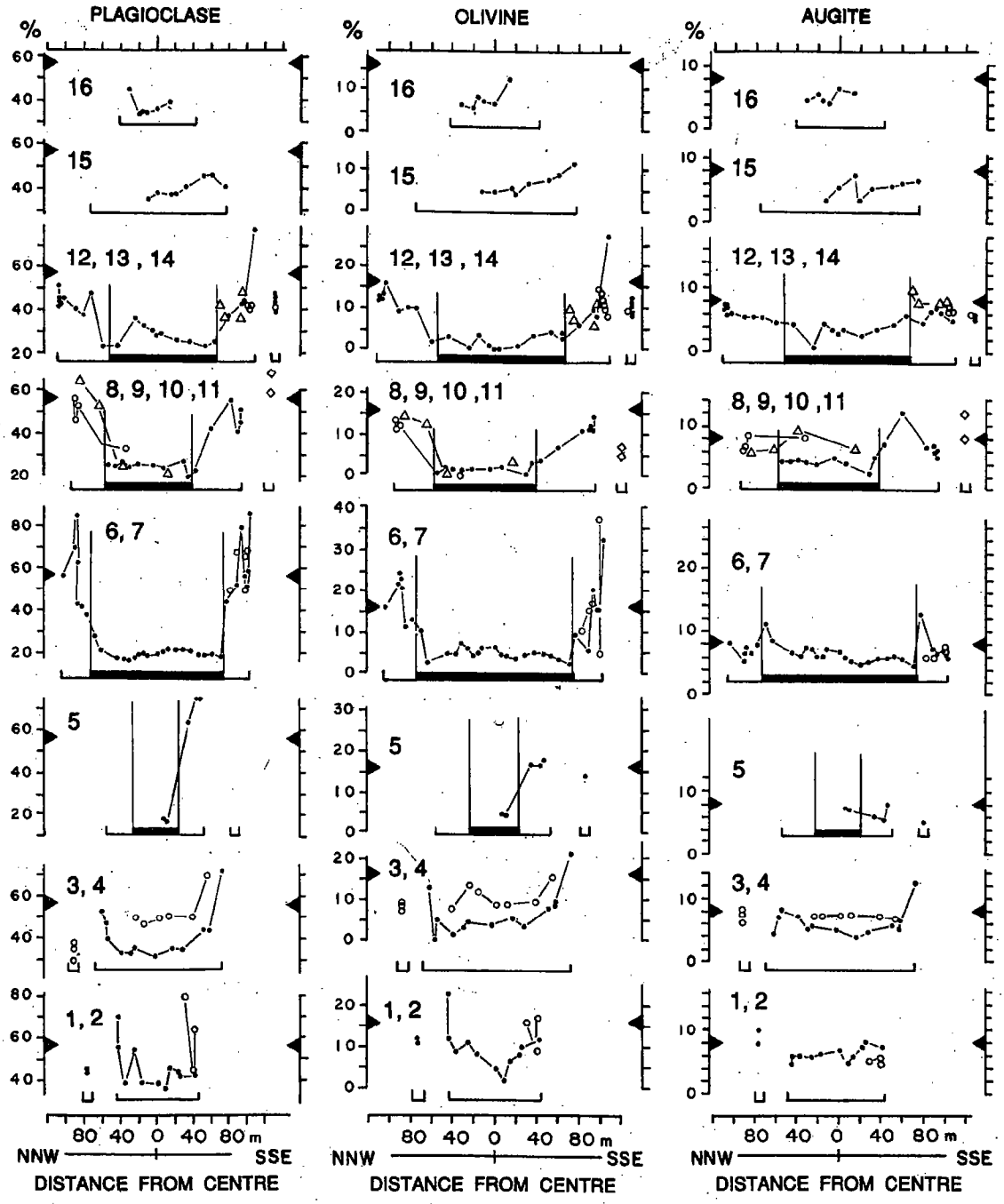

FIG. 11. Cross-section profiles for normalized Pearce element ratios of CIPW normative plagioclase, olivine, and augite (diopside). Normalized ratios are of the form $[A/Z]Z_0$. CIPW normative abundances are used for A. The variable, Z, is given by an incompatible element and Z_0 is the incompatible element content in the parental magma estimated by the chilled margin sample from traverse 7. PER values were calculated using four different incompatible elements and the results were averaged as follows (using plagioclase as an example):
Normalized

$$\mathrm{PER} = \mathrm{Plag}[\mathrm{K}_0/\mathrm{K} + \mathrm{Zr}_0/\mathrm{Zr} + \mathrm{Y}_0/\mathrm{Y} + \mathrm{Ba}_0/\mathrm{Ba}].$$

Values used for K_0, Zr_0, Y_0, and Ba_0 are 6400, 81, 23, and 624 ppm, respectively. The thick bar locates Unit 2 whereas the horizontal bracket gives the full dyke width and schematically locates the mini-dykes. The mini-dyke data from traverse 4 include samples from a mini-dyke cutting the interior of the main dyke. The arrowheads on the vertical axes locate the estimated parental composition. Circles were used for traverses 2, 4, 6, and 11, triangles for traverses 8 and 12, and diamonds for traverse 9. Dots were used to locate data from all other traverses.

accumulate on the 'hanging wall' (south) side, whereas more dense phases concentrate on the 'foot wall' (north) side. Figure 10 shows that although the mafic minerals accumulated towards the north wall, the PER-plagioclase pattern is flat, which means that plagioclase did not actually 'move' with respect to the residual liquid. This surprising result is not apparent from the non-PER diagram and illustrates the utility of the PER approach for quantitative petrology. There are several other asymmetric features presumably related to the dip of the dyke at traverse 7. The Unit 1b zone is narrower, the compositional gradient between Units 1b and 2 is sharper and the synformal foliation of Unit 2 is steeper on the south side than on the north side (Fig. 2).

REGIONAL VARIATION

Most of the patterns observed in traverse 7 (Fig. 10) apply to the dyke as a whole (Fig. 11). Overall, PER abundances of plagioclase and olivine (but not augite) tend to decrease towards the interior, indicating fractional loss of these minerals (Fig. 11). Unit 2 rocks are the most depleted, but interior Unit 1 rocks are also, on average, slightly depleted. The Mg:Fe ratios of olivine and augite also decrease from the dyke margin inwards (Ernst, 1989), also indicating that interior rocks are more evolved.

Although Unit 2 tends to vary smoothly from one sample to the next, Unit 1 rocks from most traverses, particularly, 1, 6, 7, 10, 11, and 14, show irregular profiles marked by abrupt 'jumps', which suggest both multiple intrusion and local cumulates.

Along-dyke trends in Unit 1

The scatter in the compositions of olivine, augite, and feldspar precludes identification of along-dyke trends (Ernst, 1989). However, Unit 1 samples along the dyke within 30 m of the margin (but excluding those from mini-dykes) exhibit a weak increase in incompatible element abundance towards the northeast along the dyke (Ernst, 1989). Ba and La are given as examples in Fig. 12. Many samples between 10 and 30 m away from the margin are probably cumulates (on chemical criteria) and hence are not representative of liquid compositions. The remaining samples from within 10 m of the margin, mostly non-cumulates, indicate an increase in incompatible element content towards the northeast corresponding to ~30% crystallization. The PER-plagioclase of the same samples (Fig. 11) shows an erratic decrease from 60–70% to 40% from the southwest end of the dyke towards the northeast.

The increase in incompatible element abundance and decrease in PER-plagioclase abundance towards the northeast can be interpreted in terms of a northeast-moving magma evolving *en route* by side-wall fractionation (e.g., Irving, 1980). In other words, as minerals crystallize on the walls, the residual northeast-moving magma in the interior becomes progressively more evolved (Irving, 1980; Platten & Watterson, 1987; Cadman *et al.*, 1990).

Along-dyke variation in the mini-dykes is more scattered, perhaps indicating that the mini-dykes were not exclusively fed by the chilled margin magma, but were, in places, fed by a more evolved Unit 1 magma from the dyke interior.

Along-dyke trends in Unit 2 data

The composition of Unit 2 also varies systematically along the dyke. FeO, MgO, and TiO_2 contents decrease towards the northeast, whereas Al_2O_3 content increases towards the northeast; these trends are statistically significant (Ernst *et al.*, 1987; Ernst, 1989). Such

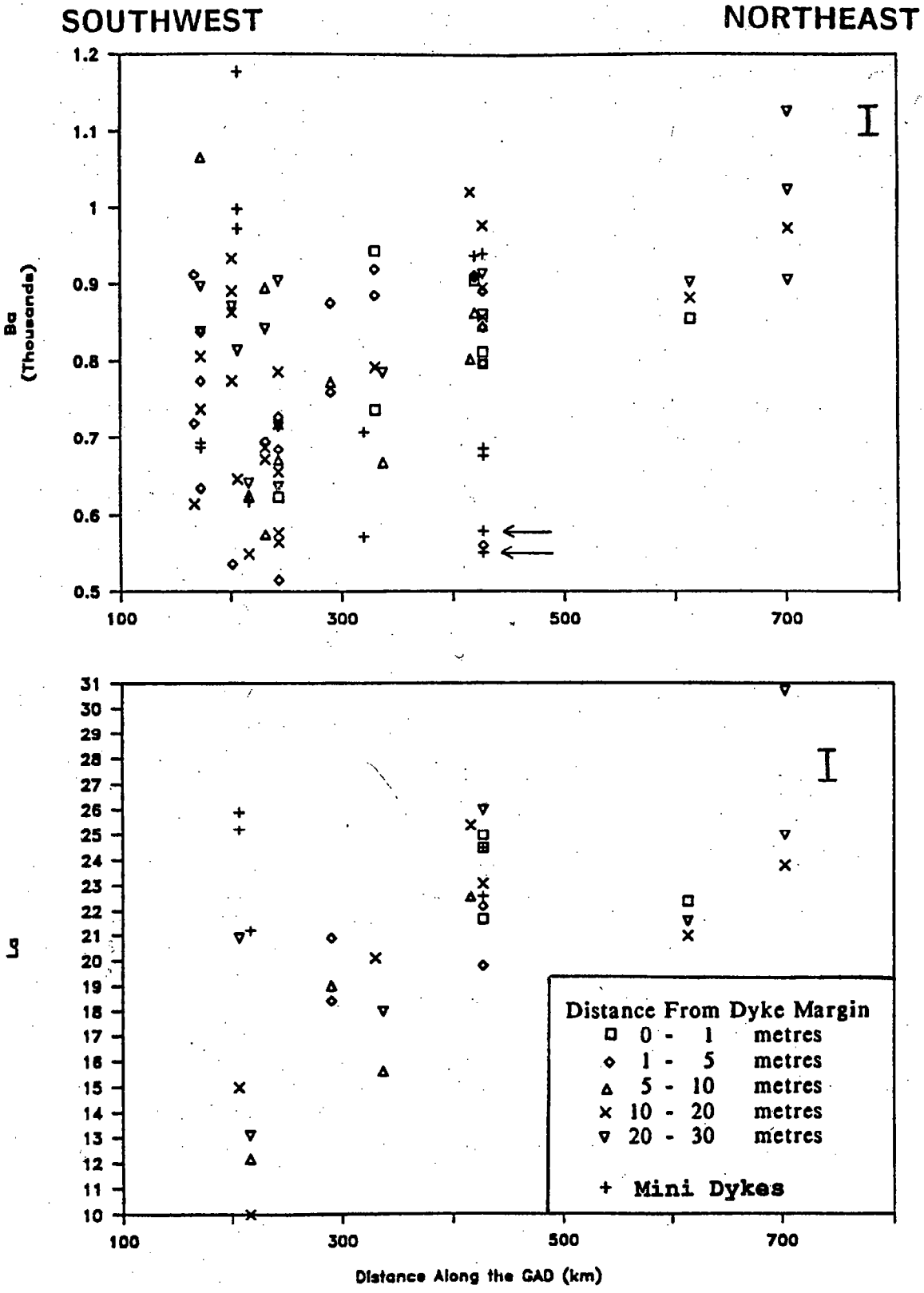

FIG. 12. Along-dyke variation in the incompatible element chemistry of Unit 1 samples. The length of the error bar equals the 2 S.D. analytical uncertainty. Two data points (marked by arrows) on the Ba graph are from mini-dykes which were probably affected by *in situ* contamination. Horizontal distances measured from Lake Superior.

patterns are consistent with a decrease in the proportion of mafic silicates (olivine, augite, and Fe–Ti oxides) to plagioclase towards the northeast (Ernst, 1989). Figure 11 displays an SSW to NNE increase in the PER abundance of plagioclase from 15% to almost 30%, and a corresponding minimal decrease in olivine, augite, and titanomagnetite and ilmenite (Ernst, 1989). No along-dyke gradient can be demonstrated in Unit 2 mineral compositions because of the large range of variation in each individual sample (Ernst, 1989).

The observed compositional pattern may correspond to a genuine horizontal gradient in mineral abundances or to an oblique section through the dyke such that a vertical zonation appears as a longitudinal gradient. Because only one section through the dyke is exposed, it is difficult to choose between these two models. The possibility of a deeper exposure level at the southwest end of the dyke is discussed below.

Mass-balance considerations

It is possible to use the graphs in Fig. 11 to make rough mass-balance calculations of the 'mineral budget' for the GAD as a whole. Estimates can be made for each mineral type as to whether fractional loss in some part of the GAD is balanced by mineral accumulation in other parts of the GAD. Strictly speaking, this 'mineral budget' applies only to the present level of exposure of the GAD. Nevertheless, this exercise yields some insights into the overall crystallization history of the dyke. This analysis employs normalized PER diagrams, which means that the data are normalized by conserved element abundance and the parental magma composition.

$$\mathrm{PER}_N(A) = Z_0(A/Z)$$

where A is the mineral (e.g., CIPW plagioclase), Z is an incompatible element, and Z_0 is the incompatible element abundance of the parental magma (approximated by the chilled margin composition at traverse 7). Only the parental magma composition will total 100%; all other samples will have differing totals depending on absolute mineral loss or accumulation relative to the parent.

The average composition of Unit 1 can be approximated by averaging over the PER values for all Unit 1 samples. Although Unit 1 profiles are fairly irregular (Fig. 11), the average PER values for all samples are 48% (±26%; 2 S.D.) plagioclase, 11% (±12%) olivine, and 7% (±3%) augite; these values are similar to the estimate of the parental magma abundances of about 57%, 17%, and 9% respectively. (The balance to 100% consists of ilmenite, titanomagnetite, and apatite.) Therefore, Unit 1 rocks show an overall quantitative balance between mineral losses (through fractionation) and gains (as cumulates), implying closed-system behaviour. However, the relationship between Units 1 and 2 is dramatically different. The average Unit 2 abundances are 22% (±8%) plagioclase, 3% (±4%) olivine, and 5% (±3%) augite. Derivation of Unit 2 from a parental Unit 1 magma requires substantial loss of available plagioclase [60% = 100 × (57 − 22)/57] and olivine [80% = 100 × (17 − 3)/17] components and less loss of titanomagnetite and ilmenite (Ernst, 1989). The loss of such minerals is not balanced by any corresponding cumulates anywhere along the present exposure level of the dyke. Either these fractionated minerals were carried to deeper exposure levels, or, alternatively, Unit 2 magma was generated elsewhere.

MODELLING OF MINERAL CHEMISTRY

A plot of olivine composition (expressed as *Fo*-number) vs. whole-rock Ba abundance yields useful information about the evolution of the GAD magma. The data in Fig. 13 show

WHOLE-ROCK Ba (ppm)

FIG. 13. Plo
number. The
liquid comp
(0% crystall

an increa
observed
incompat
numbers
olivine c
considere
(i.e. 0% c
By mo
correlate
additiona
chemistr
has cryst
with feld
can be c
Other
compara
rich in b
Skaerga

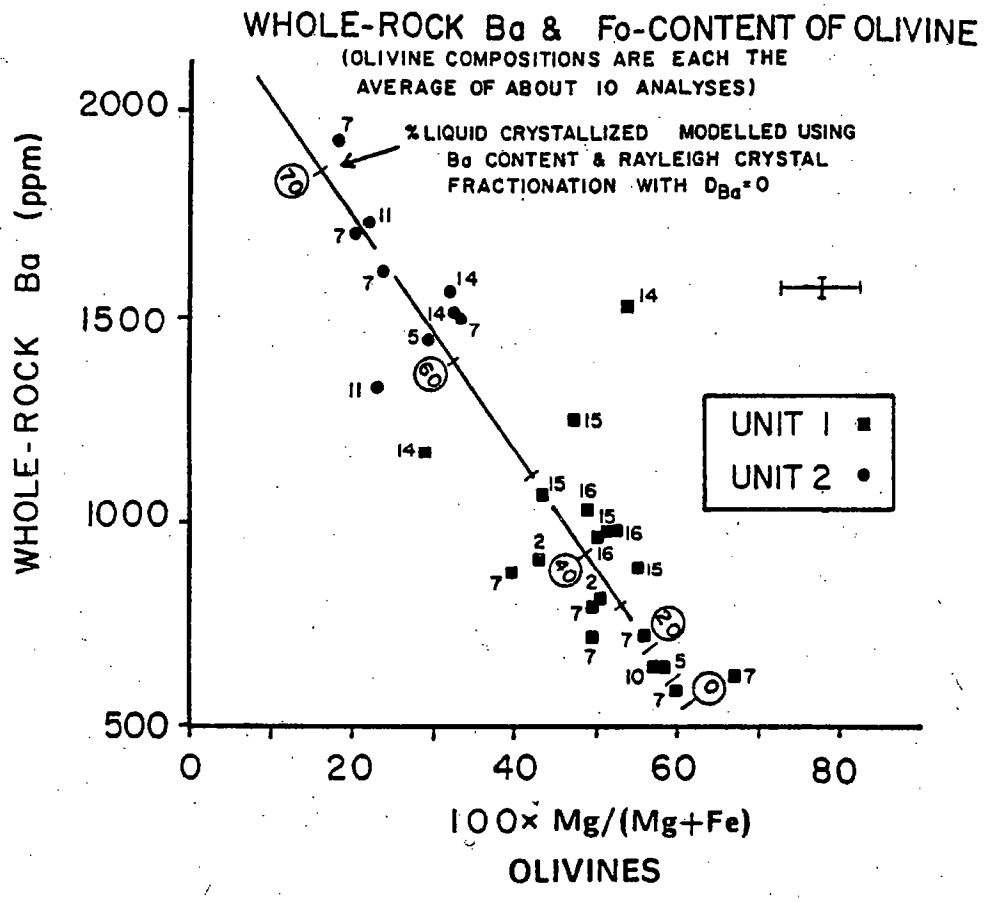

FIG. 13. Plot of whole-rock Ba concentrations and olivine compositions. Each sample is labelled by its traverse number. The circled numbers mark the degree of fractionation (percent liquid crystallized). All samples represent liquid compositions except for three cumulate samples which are all located near the parental magma composition (0% crystallized) and thus exert no control over the location of the fitted line. Cross indicates average ±2 S.D. analytical uncertainty in the data.

an increase in the Ba content as olivine becomes increasingly iron rich. The same pattern is observed using other incompatible elements instead of Ba. Given that Ba behaved as an incompatible element during crystallization of the GAD parental magma, the circled numbers in Fig. 13 chart the degree of (Rayleigh) fractional crystallization as a function of olivine composition. The Ba content of the chilled margin sample from traverse 7, considered to be a reasonable estimate of the Ba content of the parental magma, is labelled 0 (i.e. 0% crystallized) in Fig. 13.

By monitoring the degree of fractionation using Ba, Unit 1 olivine chemistry can be correlated with 0–50% fractional crystallization of the assumed parental magma. An additional 20% of fractional crystallization correlates with olivines of Unit 2. Olivine chemistry can therefore be calibrated in terms of the percentage of the parental magma that has crystallized. The covariation of olivine mineral chemistry with that of augite and also with feldspar (Figs. 14A and 14B) implies that the composition of the main mineral phases can be calibrated in terms of the degrees of crystallization of the parent magma.

Other bodies, such as Skaergaard and Kiglapait, have olivines with compositional ranges comparable with those of the GAD. Coexisting augites, however, are distinctly more iron rich in both of these complexes than those of the GAD (Fig. 15). The high Fe content of Skaergaard olivines has been attributed to re-equilibration with an Fe-rich intercumulus

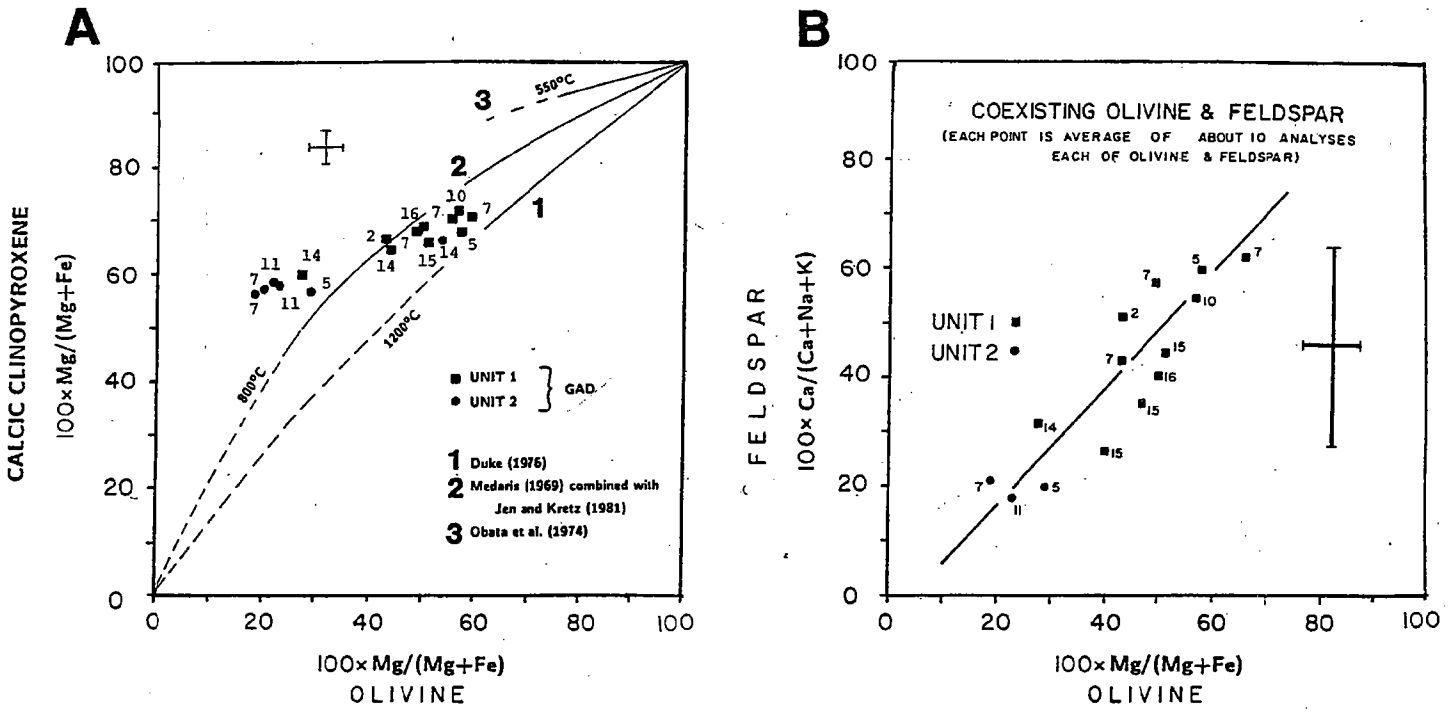

FIG. 14. Plot of coexisting olivine, augite, and feldspar compositions. (A) Olivine vs. augite. Each data point is an average of ~10 analyses each of olivine and augite. Samples are labelled by traverse number. *mg*-number = [100 × Mg/(Mg+Fe)]. These data are in molecular amounts. Isotherms are for the Mg/(Mg+Fe) compositions of coexisting olivine and calcic clinopyroxene. The 1200 °C data are from Duke (1976). The 800 °C curve is determined by combining data for Mg/Fe ratios in coexisting olivine–orthopyroxene (Medaris, 1969) with Mg/Fe ratios of coexisting orthopyroxene–clinopyroxene (Jen & Kretz, 1981). The 550 °C isotherm is from Obata *et al.* (1974). The location of these isotherms was determined by R. Kretz (pers. comm., 1989). Isotherms marked with a solid line are well constrained by data. Those with a dashed line are speculative. Cross gives an estimated ±2 S.D. uncertainty in data estimates and in the location of the isotherms. (B) Olivine vs. feldspar. These data are in molecular amounts. Each sample is labelled by its traverse number. Orthoclase analyses from evolved Unit 1 rocks were not used in computing feldspar averages. Cross indicates average ±2 S.D. dispersion about sample averages.

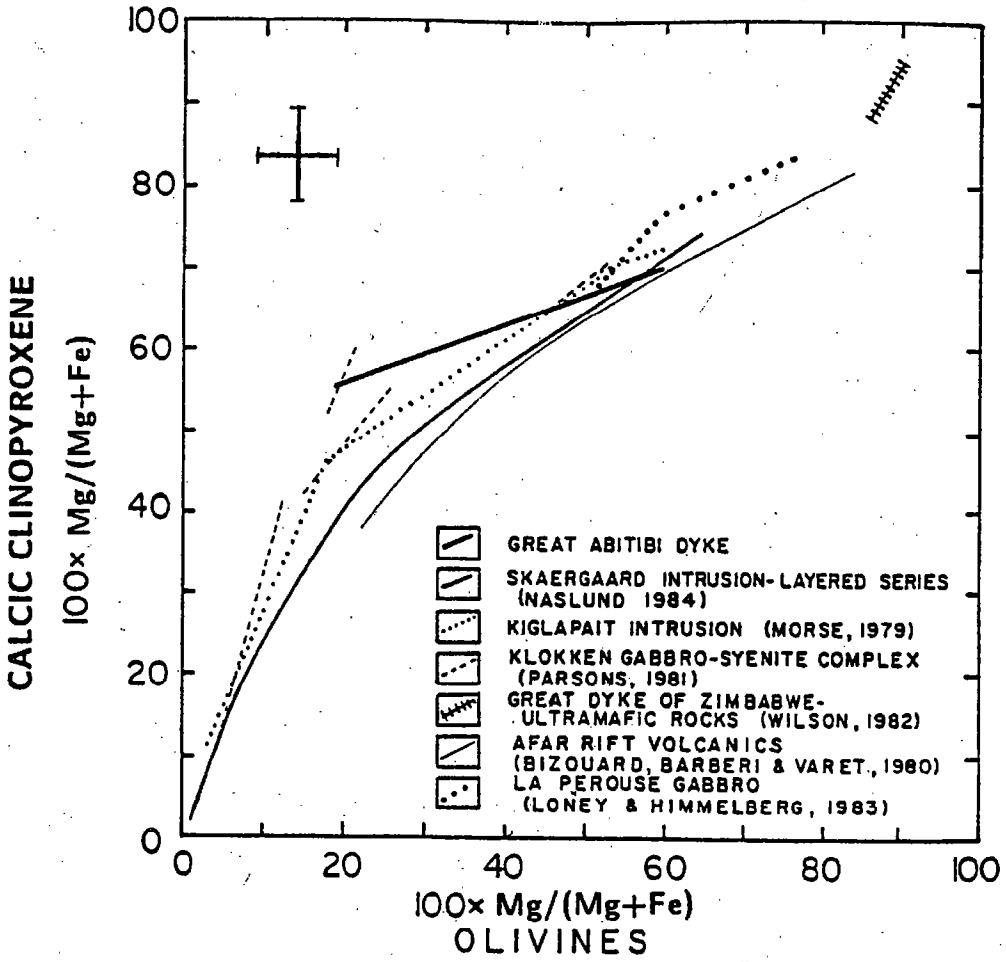

FIG. 15. Comparison of olivine–calcic clinopyroxene compositions from the GAD with those of other gabbroic bodies. Some uncertainty results from differences in the way the *En*-number of calcic clinopyroxene was calculated. In some studies Fe total was used, whereas in other cases, Fe^{2+} was used. The resulting differences in *En*-number fall within the ±2 S.D. spread of the data as given by the cross.

liquid (Naslund, 1984), but this is considered unlikely during the evolution of the GAD because such an Fe-rich intercumulus liquid would need to have (a) affected olivines to a greater degree than augites, (b) had access to all parts of the dyke (both Unit 1 and 2), and (c) caused greater iron enrichment towards the dyke interior.

The data in Fig. 14 can be attributed to variation in equilibrium temperatures. The Mg/Fe distribution between coexisting olivine and augite can be used as a geothermometer (Powell & Powell, 1974), taking into account the uncertainties noted by Wood (1976) and Parsons (1981). Preliminary isotherms were constructed using available experimental and natural data (Fig. 14). The 1200 °C and 550 °C isotherms were constructed using Ol:Cpx equilibrium data and the 800 °C isotherm was defined using combined Opx:Cpx and Opx:Ol equilibrium data. On the basis of these isotherms it appears that the Unit 1 data fall between the 1200 °C and 800 °C isotherms and that Unit 2 samples equilibrated at a temperature below 800 °C, perhaps as low as 550 °C. Comparison with relevant liquidus and solidus temperatures from Hawaiian tholeiitic lavas (Carmichael *et al.*, 1974) and the Klokken Gabbro–Syenite Complex, southern Greenland (Parsons, 1981) suggests that thermal equilibrium was attained late in the cooling history of Units 1 and 2. The GAD data in Fig.

amounts. Each sample is labelled by its traverse number. Orthoclase analyses from evolved Unit 1 rocks were not used in computing feldspar averages. Cross indicates average ±2 S.D. dispersion about sample averages.

14 were based on average values from several olivine or augite grains spread over a few centimetres. That compositional differences between grains often exceed the variation (zonation) within individual grains (Table 2) indicates that the pattern in Fig. 14 is primarily controlled by the temperature of crystallization and not by subsequent re-equilibration.

The Fe–Ti oxides provide yet another way of evaluating the cooling history of the GAD magma. Oxygen fugacities and equilibrium temperatures were obtained for the GAD using coexisting titanomagnetite and ilmenite compositions (Buddington & Lindsley, 1964; Spencer & Lindsley, 1981) according to the method of Ghiorso & Sack (1991), using the computer program supplied by M. S. Ghiorso. Analyses of composite grains of titanomagnetite and patches of ilmenite (probably produced by subsolidus exsolution) from 10 samples indicate a positive correlation between f_{O_2} and T, with an average temperature between 675 and 750°C and f_{O_2} of between 10^{-17} and 10^{-19} bars. Unit 1 and 2 data separate to higher and lower temperatures, respectively. The Fe–Ti oxide temperatures probably record exsolution of ilmenite patches from originally homogeneous titanomagnetite grains. As compositional equilibrium was reached among the Fe–Ti oxides it appears that f_{O_2} followed the quartz–fayalite–magnetite (QFM) buffer curve considered typical of most terrestrial basalts [Basaltic Volcanism Study Project (BVSP, 1981, pp. 371–5].

ORIGIN OF THE PARENTAL MAGMA

We have shown earlier that all parts of the dyke can be derived by liquid–crystal fractionation from a common parental magma similar in composition to a chilled margin sample from traverse 7. The *mg*-number [molar $100 \times Mg/(Mg+Fe)$], and Mg, Ni, and Cr contents of this parental magma (Table 3) are too low for the magma to have been in equilibrium with mantle olivines (e.g., BVSP, 1981, pp. 409–32) and therefore the parental magma cannot be considered a primary mantle melt.

Rocks of the GAD exhibit a small positive Eu anomaly superimposed on an otherwise smooth, straight, and consistently light REE-enriched pattern (Fig. 16). The REE patterns are sub-parallel, have a chondrite-normalized (cn) slope $(La/Yb)_{cn}$, of $8{\cdot}5 \pm 1{\cdot}0$ (2 S.D.) and the abundances vary by more than a factor of three. La_{cn} ranges between 40 and 120 and Yb_{cn} between 5 and 15. If the parental magma was produced by mainly olivine fractionation from the primary mantle magma (a model consistent with the low *mg*-number, Ni, and Cr values) then the REE slope of the parental magma should match that of the primary melt (Cox *et al.*, 1979; Hanson, 1980). A light REE-enriched pattern (Fig. 16) is consistent with low degrees (a few percent) of partial melting of a garnet lherzolite mantle with garnet left as a residual phase (e.g., Gast, 1968), or partial melting of a metasomatized mantle (e.g., Nielson & Noller, 1987).

The REE data from the GAD, including those from chilled margins and mini-dykes, exhibit a slight positive Eu anomaly, i.e., $Eu/Eu^* > 1$ (Fig. 16), a result that could be explained by accumulation of the plagioclase phenocrysts observed in all chilled margin and mini-dyke samples. However, the textural observations demonstrate that plagioclase phenocrysts in at least one case must have grown *in situ*; a mini-dyke cutting Unit 1 rocks at traverse 4 contains no plagioclase phenocrysts in the most chilled portion, but inwards from the chill plagioclase phenocrysts appear and increase in both size and abundance as the groundmass grain size increases. Phenocrysts which grew *in situ* cannot cause an Eu anomaly.

Values for 'excess' plagioclase in the chilled samples can be calculated from the Eu anomaly and compared with observed phenocryst abundances (Table 7). If the calculated excess of plagioclase exceeds the observed abundance of plagioclase phenocrysts, then the

FIG.
norm
Sam
suite
unce
(Eu/
Unit

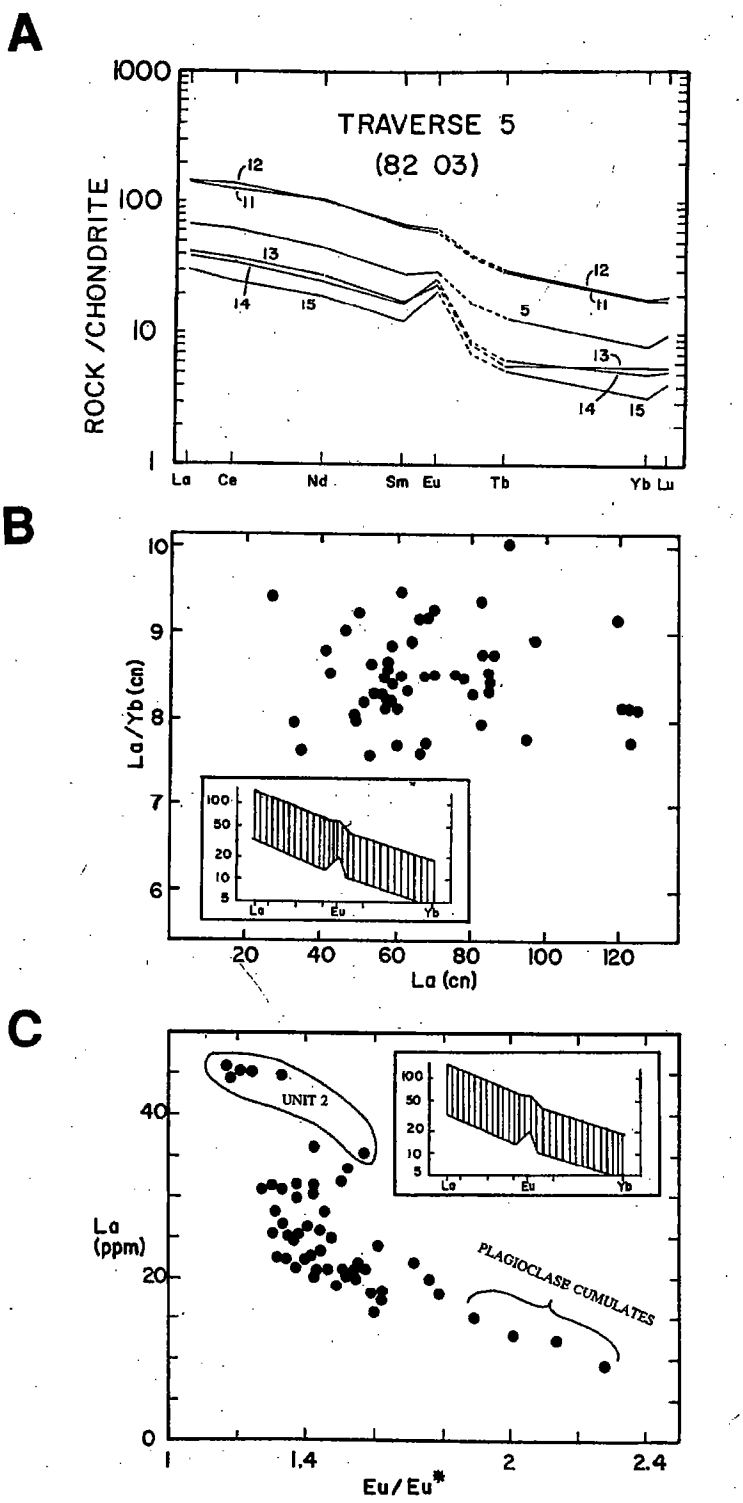

FIG. 16. Rare earth element data from the GAD. Rare earth abundances are chondrite-normalized using the normalization factors of Taylor (1980). (A) Data from traverse 5. Samples 13, 14, and 15 are plagioclase cumulates. Sample 5 is from a mini-dyke sample of Unit 1. Samples 11 and 12 are from Unit 2. (B) Data from a representative suite of 53 samples. cn—chondrite-normalized. Inset shows the range of REE data. The average 2 S.D. analytical uncertainty for La/Yb (cn) is 1 and for La (cn) is 5. Both Unit 1 and 2 data are plotted. (C) La vs. Eu anomaly (Eu/Eu*). Eu* is Eu value interpolated from values of adjacent trivalent REEs. Inset shows range of REE data. Unit 2 data are enclosed by a line. The average 2 S.D. analytical uncertainty for La is 1·5, and for Eu/Eu* is 0·1.

TABLE 7

Evaluation of origin of Eu/Eu anomaly in chilled samples from main dyke and mini-dykes*

Sample no.	*Traverse no.*	*Analyzed Eu/Eu**	*Plagioclase phenocrysts (calculated)* $K_D(Eu)=1$ $K_D(Eu^*)=0$	$K_D(Eu)=2$ $K_D(Eu^*)=0$	$K_D(Eu)=1$ $K_D(Eu^*)=0{\cdot}1$	*Plagioclase phenocrysts (point-counted)**
8204-07	4	1·40	29% (wt. %)	16%	32%	5·4% (vol. %)†
8204-19	4	1·38	28%	16%	31%	4·8%
8207-03	14	1·71	42%	26%	46%	5·3%
8207-05	14	1·30	23%	13%	26%	7·3%
8207-13	14	1·47	32%	19%	36%	5·8%
8208-09	15	1·31	24%	13%	26%	3·3%

* Point-counted on slab surfaces of samples. For each, a minimum of 1000 points were counted over an area of at least 12·5 cm^2.

† Conversion between vol. % and wt. % will not change the conclusion that the calculated phenocryst content is much larger than the observed phenocryst content.

observed Eu anomaly is at least partially characteristic of the magma and not due to plagioclase accumulation. Using a reasonable range of values for K_D of Eu and Eu* (Drake & Weill, 1975; Cox *et al.*, 1979), calculations show that at least 13 and perhaps 46 wt.% plagioclase enrichment is implied by the range in the size of Eu anomaly in chilled margin samples, an amount significantly larger than the observed abundance of plagioclase phenocrysts, which is typically $\sim 5 \pm 1$ vol.%. The plagioclase also shows no evidence of resorption. It can therefore be concluded that the positive Eu anomaly in chilled margin and mini-dyke samples is not due to phenocryst accumulation *in situ*, and is probably characteristic of the parental magma.

Spidergrams

Normalized spidergrams from the GAD which represent the parental composition (Fig. 6) are compared with reference spidergrams from mid-ocean ridge basalt (MORB), ocean island basalt (OIB), crustally contaminated continental flood basalt (CFB), and island arc basalt (IAB) (Fig. 17). OIB spidergrams (e.g., BVHO-1) as well as crustally uncontaminated CFB spidergrams (not shown) have a similar concave downward pattern (Thompson *et al.*, 1984) and both can be considered within-plate basalts (WPBs). Thompson

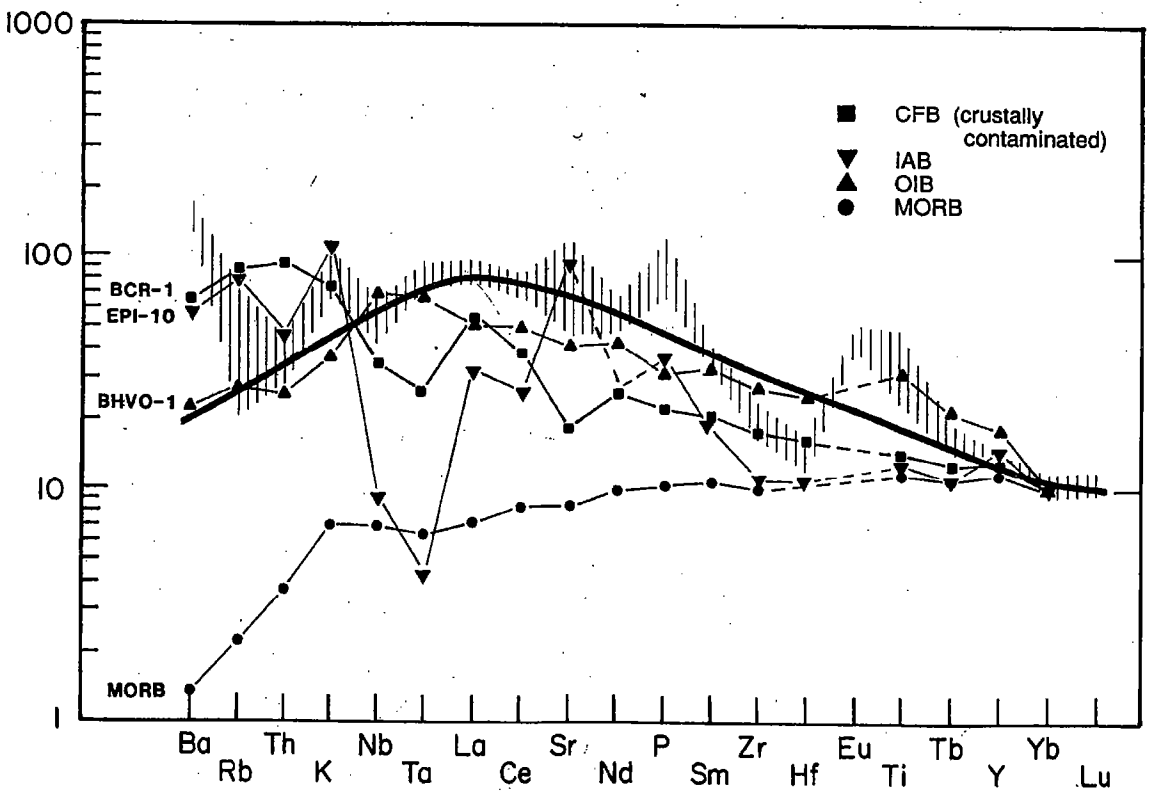

FIG. 17. Comparison of doubly normalized GAD spidergrams (Fig. 6) with those from various settings (Thompson *et al.*, 1983). The vertically hatched data represent the 1 S.D. envelope of the doubly normalized data from the GAD. The spidergram from each sample has been shifted up or down so that its Y value equals 15. BCR-1 is a sample from the Columbia River Plateau basalts and represents crustally contaminated continental flood basalts (CFB). BHVO-1 is a basalt from Kilauea, Hawaii, and represents a typical ocean island basalt (OIB) pattern, and MORB is a typical mid-ocean ridge basalt. EPI-10 is a typical island arc basalt (IAB) from the New Hebrides (Thompson *et al.*, 1984). BCR-1 and BHVO-1 are also international analytical standards. A smooth line (bold and unlabelled) is drawn through the GAD data and has the concave downward shape typical of OIBs (Thompson *et al.*, 1984).

et al. (1983) suggested that OIBs and CFBs originate from the same mantle reservoir although CFBs can be contaminated during passage through continental crust. [Also, see discussion of Duncan (1987) and Marsh (1987) on the trace element characteristics of CFBs.] Crustally contaminated CFBs, such as BCR-1, typically exhibit an overall linear spidergram which is enriched in Ba, Rb, Th, K, and the light REEs, but is unchanged or slightly depleted in Nb, Ta, P, Zr, Hf, Ti, and Y relative to uncontaminated CFBs (Thompson *et al.*, 1984). Island arc basalts (e.g., EPI-10) have a distinctive Nb–Ta trough (Thompson *et al.*, 1984), whereas MORBs are characterized by a pattern of decreasing abundance towards the left side of the spidergram. The GAD spidergrams have different shapes from those for contaminated CFBs or MORBs. Rocks of the GAD have a slight Nb trough but no Ta anomaly and are thus unlike IABs. The average spidergram from the GAD is most similar to that of WPBs (i.e., OIBs and uncontaminated CFBs), a conclusion similar to that based on various discriminant diagrams. Non-cumulate GAD samples plot in WPB fields on the F1–F2 diagram based on major elements (Pearce, 1976), the log Zr vs. log Zr/Y diagram (Pearce & Norry, 1979), and the ternary Ti–Zr–Y diagram (Pearce & Cann, 1973). The parental magma of the GAD must have been unusually rich in Ti, as many non-cumulate samples also plot out of the defined fields on the ternary Ti–Zr–Y diagram towards the Ti corner. High-Ti whole-rock compositions are also consistent with the observation that augites, biotites, and titanomagnetites from the GAD are all Ti-rich varieties (Ernst, 1989).

The conclusion that the GAD has chemistry appropriate to a 'within-plate' setting is consistent with its location within the Superior Province of the Canadian Shield and its inferred coeval relationship with the intracontinental Keweenawan rift volcanism of the Lake Superior Basin. The fit of the GAD spidergrams to an idealized OIB pattern (Fig. 17) is only approximate. The positive Ba, K, P, and Eu and negative Zr, Hf anomalies present in all samples and the positive Ti and Sr anomalies in Unit 1 samples characterize the parental magma. These anomalies may have been acquired by assimilation or fractionation during magma migration through the lithosphere or may be inherited during partial melting of anomalous mantle.

DISCUSSION

Regional variation in the depth of exposure

In Unit 2 rocks, the ratio of plagioclase to mafic minerals decreases from the southwest end of the dyke towards the mid-length region. This statistically significant along-dyke variation can be explained by an oblique exposure through a vertically zoned dyke, the more dense mineral phases being concentrated at a deeper exposure level towards the southwest (Ernst *et al.*, 1987). Although the GAD remains unmetamorphosed along its entire length, the regional variation in the host rock metamorphic grade is consistent with the shallowest level of exposure being located at mid-length along the GAD (Ernst & Halls, 1983). Host rocks from the mid-length region of the dyke do not exceed greenschist facies (Fraser *et al.*, 1978), whereas towards both the southwest and northeast ends of the dyke, the host rock reaches lower amphibolite facies. The coincidence between the least metamorphosed portions of the Archean rocks of the Abitibi belt and the proposed shallowest parts of the GAD suggests that differential uplift of the Abitibi belt occurred after emplacement of the GAD at 1141 Ma, perhaps in association with the Grenville orogeny.

Additional circumstantial support for this model is given by the geometry of the GAD. In its mid-length region the GAD breaks up into en-echelon segments with a maximum offset of $\sim$1 km (Ernst, 1991). En-echelon segmentation is expected to be more pronounced at

shallower exposure levels (Pollard, 1987), and on this basis the GAD would have the shallowest level of exposure midway along its length.

The postulated variation in exposure level is gradual. Even if the cumulative change in depth was 10 km, this change in depth occurs over several hundred kilometres, and therefore, the average angle of tilting would only be a few degrees. This tilting will have had an insignificant effect on the flow fabric direction as determined by anisotropy of magnetic susceptibility data (Ernst, 1990).

Genesis of Unit 2 magma

Although Units 1 and 2 were derived from the same parental magma, the crystallization history of each unit is different. Unit 1 behaved as a closed system, such that fractional losses from the near-margin rocks of Unit 1 are balanced by mineral accumulation (i.e., as cumulates) within the interior of Unit 1.

In contrast, the derivation of Unit 2 rocks from the parental magma requires loss of approximately half the magma volume by crystallization of plagioclase, olivine, titanomagnetite, and ilmenite. The fractionate is not observed anywhere along the present exposure level of the GAD and must have been efficiently removed. Single crystals or crystal-laden plumes may have 'rained' down the dyke-conduit, reaching depths below the present exposure level (Shirley, 1987) and leaving behind an evolved 'saddle' [Fahrig (1985); see also discussion by Kretz *et al.* (1985)] which corresponds to the magma which crystallized as Unit 2.

Alternatively, Unit 2 may have been differentiated from the parent magma elsewhere and was injected into the GAD. Injection of Unit 2 can explain various features such as (1) the sharp change in chemistry at the boundary between Units 1 and 2, (2) the gap in cooling times between Units 1 and 2 revealed by the paleomagnetic data (Ernst *et al.*, 1987; Ernst, 1989), and (3) the evidence that the parts of the dyke containing Unit 2 rocks are typically wider than parts which contain only Unit 1 rocks. Possible locations for the Unit 2 magma chamber are along, below, or above the present exposure level of the dyke. An along-dyke source can be ruled out because mapping or aeromagnetic data do not allow for any near-surface chamber of any significant size. It is possible the magma chamber is located within the Keweenawan rift at the southwest end of the dyke; but if present it must be at depth because the exposed Keweenawan rocks are younger (BVSP, 1981, p. 38). The possibility of a source at depth below the dyke cannot be evaluated directly, although any chamber is unlikely to be located at depth in granitic regions, on the basis of aeromagnetic data and evidence that granitic plutons extend to depths of 10 km (Schwarz *et al.*, 1984). A chamber could be located at depth within greenstone belts. The possibility of an overlying chamber is attractive. Many intrusions are funnel-shaped and narrow downwards into feeder dykes (Petraske *et al.*, 1978; McBirney, 1984, p. 188; Hall, 1987, p. 106). Examples are the Jimberlana Intrusion (McClay & Campbell, 1976), the Muskox Intrusion (Smith *et al.*, 1967), and the Great Dyke of Zimbabwe (Podmore & Wilson, 1987).

The synformal distribution of feldspar foliation (Fig. 2) requires some downward movement of Unit 2 magma, either downwards magma injection from an overlying chamber, or simply a minor late-stage drop in magma level, compatible with all the models for the origin of Unit 2.

Magma flow direction recorded in Unit 1 rocks

The chemical composition of Unit 1 rocks exhibits a slightly more evolved character towards the northeast end of the GAD, which may be attributed to side-wall fractionation

(Irving, 1980) of Unit 1 magma moving along a sub-horizontal trajectory towards the northeast, implying a magma source to the southwest of the dyke. A sub-horizontal trajectory for magma injection is also supported by magnetic susceptibility anisotropy measurements (Ernst *et al.*, 1987; Ernst, 1990). A similar shallow trajectory of magma emplacement has been determined for other dyke swarms. In particular, various lines of evidence including geochemical, textural, anisotropy of magnetic susceptibility, and seismic studies have demonstrated that although the flow direction of dykes can be highly variable, it is often sub-horizontal (e.g., Baer & Reches, 1987; Sigurdsson, 1987; Smith, 1987; Greenough *et al.*, 1988; Knight & Walker, 1988; Macdonald *et al.*, 1988; Greenough & Hodych, 1990). Theoretical work by Delaney (1987) and Lister & Kerr (1990) also demonstrated the feasibility of lateral mafic magma transport over substantial distances.

Relationship to the regional geology

To the southwest of the GAD (Fig. 1), the Lake Superior basin hosts a thick accumulation of Keweenawan mafic volcanic rocks and dykes with ages ranging between 1110 and 1085 Ma (Davis & Sutcliffe, 1985; Palmer & Davis, 1987; Davis & Paces, 1990). These Keweenawan rocks are ~30 Ma younger in age than the GAD, but are probably related to the same magmatic event. There are similarities between the chemical composition of the GAD and Keweenawan volcanics; both tend to be Al rich, have small positive Eu anomalies and light REE-enriched patterns, suggesting that the magma source for the GAD was within the Keweenawan rift at the southwest end of the dyke. Some dykes of the Abitibi swarm (particularly the Kipling and the GAD) fan over a narrow arc away from the Superior basin (Fig. 1), suggesting that the dykes mark a 'failed' arm associated with Keweenawan rifting (Burke & Dewey, 1973; Condie *et al.*, 1987; Fahrig, 1987).

At the northeastern end of the GAD, dykes of the Abitibi swarm fan out from a bulge in the Grenville Front that separates the Superior and Grenville Provinces (Ranalli & Ernst, 1986). The Grenville Front, northeast of this bulge, is associated with a prominent negative gravity anomaly. The gravity anomaly may be due to crustal thickening during compression, and it is possible to construct the stress trajectories within the Superior Province resulting from boundary loads associated with the Grenvillian Orogeny. The strike of the GAD and related dykes east of the Kapuskasing Structural Zone (KSZ) is everywhere normal to the direction of minimum compression (Ranalli & Ernst, 1986). The age of the GAD (1141 Ma; Krogh *et al.*, 1987) roughly coincides with a compressive phase of the Grenvillian Orogeny (e.g., Gibb *et al.*, 1983; Easton, 1986; Windley, 1986), suggesting that the GAD and related dykes were emplaced in response to a stress field associated with Grenvillian orogenesis.

The KSZ cuts across the Superior Province between Lake Superior and James Bay (Fig. 1), and marks a break along which east-verging thrusting occurred in the early Proterozoic (Percival & McGrath, 1986). The GAD is collinear with the southern boundary of the Kapuskasing Structural Zone, suggesting that emplacement of the GAD magma at 1141 Ma may have taken advantage of a pre-existing zone of weakness collinear with the southern boundary fault of the KSZ.

We propose that at 1141 Ma, upwelling asthenosphere began to impinge on the lithosphere in the Lake Superior region. The earliest effect of the upwelling was emplacement of the Abitibi dyke swarm, which by 1109–1085 Ma was fully expressed as the Keweenawan rift [isotopic evidence consistent with the upwelling model was presented by Paces & Bell (1989)]. The location of the Abitibi dykes east of the KSZ was also influenced

by (1) Grenville compression and (2) a pre-existing zone of the weakness along the extension of the southern boundary zone of the KSZ.

Relation to Gardar Province rocks

The GAD is strikingly similar in age, chemistry, and mineralogy to two of the giant dyke complexes of the Gardar Province of southern Greenland. The GAD can be matched to the gabbroic phases of both the Tugtutoq Older Giant Dyke Complex and Tugtutoq Younger Giant Dyke Complex, both emplaced at ~1150 Ma (Upton, 1987; Upton & Emeleus, 1987). The parental magma of these giant dykes represented by chilled margins was an anhydrous olivine basalt of transitional character with high Ti, P, and Ba features considered to have been inherited from a primary magma which was derived from the mantle by small degrees of partial melting involving significant amounts of fluorapatite and phlogopite. Given the compositional similarity with the GAD, a similar environment of mantle partial melting could be attributed to the GAD. In a reassembled Laurentia, the GAD is also roughly collinear with these Gardar Province dykes, providing a combined length of >2000 km.

CONCLUSIONS

The Great Abitibi Dyke (GAD) consists of two texturally and compositionally distinct units which may represent separate magma pulses. Unit 1 was emplaced first (probably as a series of multiple intrusions) and in turn was intruded by Unit 2. Unit 2 is characterized by a feldspar lamination that defines a synformal pattern with axis aligned parallel to the dyke plane and sub-horizontal plunge. Field observations reveal that the dyke generally has a near-vertical dip.

Unit 1 olivine gabbros contain plagioclase of composition $An_{68-15}Or_{0-10}$, olivine of Fo_{60-30}, and augite of En_{75-55}. Most Unit 2 samples, on the other hand, contain olivine of composition Fo_{35-20}, augite of En_{60-45}, and feldspar of $An_{40-0}Or_{5-40}$.

Modelling of the chemical data using Pearce element ratio analysis suggests that the Great Abitibi Dyke has a relatively simple history of evolution. All parts of the dyke could have been derived by fractional crystallization of mainly plagioclase and olivine (and augite in Unit 2 rocks) from the same parent magma corresponding to chilled-margin chemistry. Near-margin samples of Unit 1 become slightly more enriched in the incompatible elements towards the northeast end of the dyke and Unit 2 rocks become more plagioclase rich and olivine and augite poor towards the northeast end of Unit 2. The model most consistent with these data involves a magma source underlying the Keweenawan rift and emplacement of the parental magma along a sub-horizontal trajectory towards the northeast. Unit 1 rocks represent a range of 0–50% fractional crystallization of the parental magma. Unit 2 is more evolved and was derived from the parental magma either *in situ* through settling of crystals to deeper parts of the dyke or by differentiation in an external chamber and subsequent emplacement into the dyke. Longitudinal variation in Unit 2 chemistry may reflect a varied exposure level. Asymmetrical variation in the bulk composition of Unit 2 and possibly 1b rocks at traverse 7 is attributed to magma crystallization in an off-vertical dyke conduit.

Trace and major element discriminant diagrams as well as incompatible element spidergrams reveal that the magma-type of the GAD is a within-plate basalt (WPB) and that the parental magma is enriched in Ba, K, P, Sr, Eu, and Ti, and depleted in Zr and Hf relative to a typical OIB.

The Great Abitibi Dyke was emplaced at 1141 Ma (Krogh *et al.*, 1987), which is similar in age to Keweenawan igneous activity, the compressive phase of the Grenville Orogeny, the intrusion of carbonatites in the vicinity of the KSZ, and emplacement of the Tugtutoq Younger and Older Giant Dyke Complexes in the Gardar Province of southern Greenland. The GAD was probably emplaced as a consequence of asthenospheric upwelling associated with the Keweenawan rift, fracturing caused by Grenville compression, and weaknesses associated with the extension of the southern boundary fault of the KSZ.

ACKNOWLEDGEMENTS

The authors acknowledge advice given by Ralph Kretz and Kent Condie during R. Ernst's Ph.D. study which forms the basis of this paper. This research was partly supported by NSERC grant A7813 to K. Bell. Detailed comments by C. K. Brooks, A. E. Lalonde, S. P. Mingard, B. J. Upton, and A. H. Wilson are gratefully acknowledged, as are those by T. Peterson on a earlier version of the manuscript. Also appreciated were the discussions with B. J. Upton regarding the relationship of the GAD to the Gardar Province Dykes and R. Kretz's suggestions for relevant isotherms in Fig. 4.

REFERENCES

Allègre, C. J., Treuill, M., Minster, J-F., Minster, B., & Albarède, F., 1977. Systematic use of trace elements in igneous processes. Part 1: Fractional crystallization processes in volcanic suites. *Contr. Miner. Petrol.* **60,** 57–75.

Baer, G., & Reches, Z., 1987. Flow patterns of magma in dikes, Makhtesh Ramon, Israel. *Geology* **15,** 569–72.

Barnes, S.-J., & Gorton, M. P., 1984. Trace element analysis by neutron activation with a low flux reactor (Slowpoke-II): results for international reference rocks. *Geostandards Newslett.* **8,** 17–23.

Basaltic Volcanism Study Project (BVSP), 1981. *Basaltic Volcanism on the Terrestrial Planets.* New York: Pergamon Press, 1286 pp.

Bell, K., & Blenkinsop, J., 1987. Archean depleted mantle: evidence from neodymium and strontium initial isotopic ratios of carbonatites. *Geochim. Cosmochim. Acta* **51,** 291–7.

Bizouard, H., Barberi, F., & Varet, J., 1980. Mineralogy and petrology of Erta Ale and Boina volcanic series, Afar rift, Ethiopia. *J. Petrology* **21,** 401–36.

Brooks, C. K., 1976. The Fe_2O_3/FeO ratio of basalt analyses: an appeal for a standardized procedure. *Bull. Geol. Surv. Denmark* **25,** 117–20.

Buddington, A. F., & Lindsley, D. H., 1964. Iron–titanium oxide minerals and synthetic equivalents. *J. Petrology* **5,** 310–57.

Burke, K., & Dewey, J. F., 1973. Plume-generated triple junctions: key indicators in applying plate tectonics to old rocks. *J. Geol.* **81,** 406–33.

Cadman, A., Tarney, J., & Park, R. G., 1990. Intrusion and crystallisation features in Proterozoic dyke swarms. In: Parker, A. J., Rickwood, P. C., & Tucker, D. H. (eds.) *Mafic Dykes and Emplacement Mechanisms. Proc. 2nd Int. Dyke Conf.*, Adelaide, South Australia, 12–16 September 1990. Rotterdam: Balkema, 13–24.

Card, K. D., Percival, J. A., Lafleur, J., & Hogarth, D. D., 1981. Progress report on regional geological synthesis, Central Superior Province. In: *Current Research, Part A. Geol. Surv. Canada, Paper* **81-1A,** 77–93.

Carlson, R. W., Lugmair, G. W., & MacDougall, J. D., 1981. Columbia River volcanism: the question of mantle heterogeneity or crustal contamination. *Geochim. Cosmochim. Acta* **45,** 2483–500.

Carmichael, I. S. E., Turner, F. J., & Verhoogen, J., 1974. *Igneous Petrology.* New York: McGraw–Hill, 739 pp.

Condie, K. C., Bobrow, D. J., & Card, K. D., 1987. Geochemistry of Precambrian mafic dykes from the southern Superior Province of the Canadian Shield. In: Halls, H. C., & Fahrig, W. F. (eds.) *Mafic Dyke Swarms. Geol. Assoc. Canada Spec. Paper* **34,** 95–108.

Cox, K. G., Bell, J. D., & Pankhurst, R. J., 1979. *The Interpretation of the Igneous Rocks.* London: George Allen and Unwin, 450 pp.

Davis, D. W., & Paces, J. R., 1990. Time resolution of geologic events on the Keweenaw Peninsula and implications for development of the Midcontinent rift system. *Earth Planet. Sci. Lett.* **97,** 54–64.

—— Sutcliffe, R. H., 1985. U–Pb ages from the Nipigon plate and northern Lake Superior. *Geol. Soc. Am. Bull.* **96,** 1572–9.

Deer, W. A., Howie, R. A., & Zussman, J., 1966. *An Introduction to the Rock-Forming Minerals.* London: Longman, 528 pp.

———— 1978. *Single-Chain Silicates, Vol. 2A, Rock-Forming Minerals,* 2nd Edn. London: Longman, 668 pp.

Delaney, P. T., 1987. Heat transfer during emplacement and cooling of mafic dykes. In: Halls, H. C., & Fahrig, W. F. (eds.) *Mafic Dyke Swarms. Geol. Assoc. Canada Spec. Paper* **34,** 31–46.
Drake, M. J., & Weill, D. F., 1975. Partition of Sr, Ba, Ca, Y, Eu^{2+}, Eu^{3+}, and other REE between plagioclase feldspar and magmatic liquid: an experimental study. *Geochim. Cosmochim. Acta* **39,** 689–712.
Duke, J. M., 1976. Distribution of the period four transition elements among olivine, calcic clinopyroxene and mafic silicate liquid: experimental results. *J. Petrology* **17,** 499–521.
Duncan, A. R., 1987. The Karoo igneous province—a problem area for inferring tectonic setting from basalt geochemistry. *J. Volcanol. Geotherm. Res.* **32,** 13–34.
Easton, R. M., 1986. Geochronology of the Grenville Province. In: Moore, J. M., Davidson, A., & Baer, A. J. (eds.) *The Grenville Province. Geol. Assoc. Canada Spec. Paper* **31,** 127–73.
Ernst, R. E., 1989. The Great Abitibi Dyke, southeastern Superior Province, Canada. Unpublished Ph.D. thesis, Carleton University, Ottawa, 579 pp.
——1990. Magma flow directions in two mafic Proterozoic dyke swarms of the Canadian Shield: as estimated using anisotropy of magnetic susceptibility data. In: Parker, A. J., Rickwood, P. C., & Tucker, D. H. (eds.) *Mafic Dykes and Emplacement Mechanisms. Proc. 2nd Int. Dyke Conf.*, Adelaide, South Australia, 12–16 September 1990. Rotterdam: Balkema, 231–5.
——1991. The near-surface geometry of the Great Abitibi Dike, Superior Province, Canada. Geol. Soc. Am. Map Chart Series, MCH-071.
——Bell, K., Ranalli, G., & Halls, H. C., 1987. The Great Abitibi Dyke, Southeastern Province, Canada. In: Halls, H. C., & Fahrig, W. F. (eds.) *Mafic Dyke Swarms. Geol. Assoc. Canada Spec. Paper* **34,** 123–35.
——Fowler, A. D., & Pearce, T. H., 1988. Modelling of igneous fractionation and other processes using Pearce diagrams. *Contr. Miner. Petrol.* **100,** 12–18.
——Halls, H. C., 1983. Structural variation of Proterozoic dikes in the central Superior Province—a possible reflection of post-Archean shield deformation. In: Ashwal, L. D., & Card, K. D. (eds.) *Workshop on a Cross-Section of Archean Crust.* LPI Tech. Rep. 83-03. Lunar and Planetary Institute, Houston, TX, 42–6.
Fahrig, W. F., 1985. The tectonic settings of continental diabase dyke swarms: failed arm and early passive margin. In: *Abstract Volume, Int. Conf. Mafic Dyke Swarms*, University of Toronto, Toronto, Ontario, 4–7 June 1985, 42–3.
——1987. The tectonic settings of continental mafic dyke swarms: failed arm and early passive margin. In: Halls, H. C., & Fahrig, W. F. (eds.) *Mafic Dyke Swarms. Geol. Assoc. Canada Spec. Paper* **34,** 331–48.
——West, T. D., 1986. Diabase dykes of the Canadian shield. Geol. Surv. Canada, Map 1627A.
Fraser, J. A., Heywood, W. W., & Mazurski, M. A., 1978. Metamorphic map of the Canadian Shield. Geol. Surv. Canada, Map 1475A.
Gast, P. W., 1968. Trace element fractionation and the origin of tholeiitic and alkaline magma types. *Geochim. Cosmochim. Acta* **32,** 1057–86.
Ghiorso, M. S., & Sack, R. O., 1991. Thermochemistry of oxide minerals. In: Lindsley, D. H. (ed.) *Oxide Minerals: Petrologic and Magnetic Significance. Miner. Soc. Am. Rev. Miner.* **25,** 221–64.
Gibb, R. A., Thomas, M. D., Lapointe, P. L., & Mukhopadhyay, M., 1983. Geophysics of proposed Proterozoic sutures in Canada. *Precambrian Res.* **19,** 349–84.
Goodwin, A. M., Ambrose, J. W., Ayers, L. D., Clifford, P. M., Currie, K. L., Ermanovics, I. M., Fahrig, W. F., Gibb, R. A., Hall, D. H., Innes, M. J. S., Irvine, T. N., MacLaren, A. S., Norris, A. W., & Pettijohn, F. J., 1972. The Superior Province. In: Price, R. A., & Douglas, R. J. W. (eds.) *Variations in Tectonic Styles in Canada. Geol. Assoc. Canada Spec. Paper* **11,** 527–623.
Greenough, J. D., & Hodych, J. P., 1990. Evidence for lateral magma injection in the Early Mesozoic dykes of eastern North America. In: Parker, A. J., Rickwood, P. C., & Tucker, D. H. (eds.) *Mafic Dykes and Emplacement Mechanisms. Proc. 2nd Int. Dyke Conf.*, Adelaide, South Australia, 12–16 September 1990. Rotterdam: Balkema, 35–46.
——Ruffman, A., & Owen, J. V., 1988. Magma injection directions inferred from a fabric study of the Popes Harbour dike, eastern shore, Nova Scotia, Canada. *Geology* **16,** 547–50.
Hall, A., 1987. *Igneous Petrology.* Harlow, Essex: Longman; and New York: John Wiley, 573 pp.
Hanson, G. N., 1980. Rare earth elements in petrogenetic studies of igneous systems. *Ann. Rev. Earth Planet. Sci. Lett.* **8,** 371–406.
Irvine, T. N., & Baragar, W. R. A., 1971. A guide to the chemical classification of the common volcanic rocks. *Can. J. Earth Sci.* **8,** 523–48.
Irving, A. J., 1980. Petrology and geochemistry of composite ultramafic xenoliths in alkalic basalts and implications for magmatic processes within the mantle. *Am. J. Sci.* **280A,** 389–426.
Jen, L. S., & Kretz, R., 1981. Mineral chemistry of some mafic granulites from the Adirondack region. *Can. Miner.* **19,** 479–91.
Johnson, W. M., & Maxwell, J. A., 1981. *Rock and Mineral Analyses,* 2nd Edn. Toronto: John Wiley, 489 pp.
Kalsbeek, F., & Taylor, P., 1986. Chemical and isotopic homogeneity of a 400 km long basic dyke in central West Greenland. *Contr. Miner. Petrol.* **93,** 439–48.
Knight, M. D., & Walker, G. P. L., 1988. Magma flow directions in dikes of the Koolau complex, Oahu, determined from magnetic fabric studies. *J. Geophys. Res.* **93,** 4301–19.
Komar, P. D., 1972. Mechanical interactions of phenocrysts and flow differentiation of igneous dykes and sills. *Geol. Soc. Am. Bull.* **83,** 973–88.

Kretz, R., 1985. Calculation and illustration of uncertainty in geochemical analyses. *J. Geol. Educ.* **33,** 40–4.
——Hartree, R., Garrett, D., & Cermignani, C., 1985. Petrology of the Grenville swarm of gabbro dykes, Canadian Precambrian Shield. *Can. J. Earth Sci.* **22,** 53–71.
Krogh, T. E., Corfu, F., Davis, D. W., Dunning, G. R., Heaman, L. M., Kamo, S. L., Machado, N., Greenough, J. D., & Nakamura, E., 1987. Precise U–Pb isotopic ages of diabase dykes and mafic to ultramafic rocks using trace amounts of baddeleyite and zircon. In: Halls, H. C., & Fahrig, W. F. (eds.) *Mafic Dyke Swarms. Geol. Assoc. Canada Spec. Paper* **34,** 147–52.
Lister, U. R., & Kerr, R. C., 1990. Fluid-mechanical models of dyke propagation and magma transport. In: Parker, A. J., Rickwood, P. C., & Tucker, D. H. (eds.) *Mafic Dykes and Emplacement Mechanisms. Proc. 2nd Int. Dyke Conf.*, Adelaide, South Australia, 12–16 September 1990. Rotterdam: Balkema, 69–80.
Loney, R. A., & Himmelberg, G. R., 1983. Structure and petrology of the La Perouse gabbro intrusion, Fairweather Range, southeastern Alaska. *J. Petrology* **24,** 377–423.
Macdonald, R., Wilson, L., Thorpe, R. S., & Martin, A., 1988. Emplacement of the Cleveland Dyke: evidence from geochemistry, mineralogy and physical modelling. *Ibid.* **29,** 559–83.
Marsh, J. S., 1987. Basalt geochemistry and tectonic discrimination within continental flood basalt provinces. *J. Volcanol. Geotherm. Res.* **32,** 35–49.
McBirney, A. R., 1984. *Igneous Petrology.* San Francisco: Freeman, Cooper, 509 pp.
McClay, K. R., & Campbell, I. H., 1976. The structure and shape of the Jimberlana Intrusion, western Australia, as indicated by an investigation of the Bronzite Complex. *Geol. Mag.* **113,** 129–39.
Medaris, L. G., Jr., 1969. Partitioning of Fe^{2+} and Mg^{2+} between coexisting synthetic olivine and orthopyroxene. *Am. J. Sci.* **267,** 945–68.
Miyashiro, A., 1978. Nature of alkalic volcanic rock series. *Contr. Miner. Petrol.* **66,** 91–104.
Morse, S. A., 1979. Kiglapait geochemistry I: systematics, sampling and density. *J. Petrol.* **20,** 555–90.
——1980. Kiglapait mineralogy II: Fe–Ti oxide minerals and the activities of oxygen and silica. *Ibid.* **21,** 685–719.
Naslund, H. R., 1984. Petrology of the Upper Border Series of the Skaergaard Intrusion. *Ibid.* **25,** 185–212.
Nicholls, J., & Stout, M. Z., 1988. Picritic melts in Kilauea—evidence from the 1967–1968 Halemaumau and Hiiaka eruptions. *Ibid.* **29,** 1031–57.
Nielson, J. E., & Noller, J. S., 1987. Processes of mantle metasomatism; constraints from observations of composite peridotite xenoliths. In: Morris, E. M., & Pasteris, J. D. (eds.) *Mantle Metasomatism and Alkaline Magmatism. Geol. Soc. Am. Spec. Paper* **215,** 61–76.
Obata, M., Banno, S., & Mori, T., 1974. The iron–magnesium partitioning between naturally occurring coexisting olivine and Ca-rich clinopyroxene: an application of the simple mixture model to olivine solid solution. *Bull. Soc. Fr. Minér. Cristallogr.* **97,** 101–7.
Paces, J. B., & Bell, K., 1989. Non-depleted sub-continental mantle beneath the Superior Province of the Canadian Shield: Nd–Sr isotopic and trace element evidence from Midcontinent Rift basalts. *Geochim. Cosmochim. Acta* **53,** 2023–35.
Palmer, H. C., & Davis, D. W., 1987. Paleomagnetism and U–Pb geochronology of volcanic rocks from Michipicoten Island, Lake Superior, Canada: precise time calibration of the Keweenawan polar wander track. *Precambrian Res.* **37,** 157–71.
Parsons, I., 1981. The Klokken gabbro–syenite complex, South Greenland: quantitative interpretation of mineral chemistry. *J. Petrology* **22,** 233–60.
Pearce, J. A., 1976. Statistical analysis of major element patterns in basalts. *Ibid.* **17,** 15–43.
——Cann, J. R., 1973. Tectonic setting of basic volcanic rocks determined using trace element analyses. *Earth Planet. Sci. Lett.* **19,** 290–300.
——Norry, M. J., 1979. Petrogenetic implications of Ti, Zr, Y, and Nb variations in volcanic rocks. *Contr. Miner. Petrol.* **69,** 33–47.
Pearce, T. H., 1968. A contribution to the theory of variation diagrams. *Ibid.* **19,** 142–57.
Percival, J. A., & McGrath, P. H., 1986. Deep crustal structure and tectonic history of the northern Kapuskasing uplift of Ontario: an integrated petrological–geophysical study. *Tectonics* **5,** 553–72.
Petraske, A. K., Hodge, D. S., & Shaw, R., 1978. Mechanics of emplacement of basic intrusions. *Tectonophysics* **46,** 41–63.
Platten, I. M., & Watterson, J., 1987. Magma flow and crystallization in dyke fissures. In: Halls, H. C., & Fahrig, W. F. (eds.) *Mafic Dyke Swarms. Geol. Assoc. Canada Spec. Paper* **34,** 65–73.
Podmore, F., & Wilson, A. H., 1987. A reappraisal of the structure, geology and emplacement of the Great Dyke, Zimbabwe. *Ibid.* 317–30.
Pollard, D. D., 1987. Elementary fracture mechanics applied to the structural interpretation of dykes. *Ibid.* 5–24.
Powell, M., & Powell, R., 1974. An olivine–clinopyroxene geothermometer. *Contr. Miner. Petrol.* **48,** 249–63.
Ranalli, G., & Ernst, R. E., 1986. The Abitibi dyke swarm: a consequence of Superior–Grenville interaction? *Tectonophysics* **121,** 357–63.
Rollinson, H. R., & Roberts, C. R., 1986. Ratio correlations and major element mobility in altered basalts and komatiites. *Contr. Miner. Petrol.* **93,** 89–97.
Russell, J. K., & Nicholls, J., 1988. Analysis of petrologic hypotheses with Pearce element ratios. *Ibid.* **99,** 25–35.
——Stanley, C. (eds.), 1990*a*. *Theory and Application of Pearce Element Ratios to Geochemical Data Analysis. Geol. Assoc. Canada Short Course* **8,** 315 pp.

———1990*b*. A theoretical basis for the development and use of chemical variation diagrams. *Geochim. Cosmochim. Acta* **54,** 2419–31.
Schwarz, E. J., Laverdue, L., Losier, L., & Poterlot, E., 1984. Preliminary gravity, magnetic and refraction seismic results from the Abitibi belt, Quebec. *Current Res. Geol. Surv. Canada Paper* **84-1A,** 239–46.
Shirley, D. N., 1987. Differentiation and compaction in the Palisades Sill, New Jersey. *J. Petrology* **28,** 835–65.
Sigurdsson, H., 1987. Dyke injection in Iceland: a review. In: Halls, H. C., & Fahrig, W. F. (eds.) *Mafic Dyke Swarms. Geol. Assoc. Canada Spec. Publ.* **34,** 55–64.
Smith, C. H., Irvine, T. N., & Findlay, D. C., 1967. Geological maps of the Muskox Intrusion, Geol. Surv. Canada, Map Sheets 1213A and 1214A.
Smith, R. P., 1987. Dyke emplacement at Spanish Peaks, Colorado. In: Halls, H. C., & Fahrig, W. F. (eds.) *Mafic Dyke Swarms. Geol. Assoc. Canada Spec. Publ.* **34,** 47–54.
Spencer, K. J., & Lindsley, D. H., 1981. A solution model for coexisting iron–titanium oxides. *Am. Miner.* **66,** 1189–201.
Stanley, C. R., & Russell, J. K., 1989. Petrologic hypothesis testing with Pearce element ratio diagrams: derivation of diagram axes. *Contr. Miner. Petrol.* **103,** 78–89.
Streckeisen, A., 1976. To each plutonic rock its proper name. *Earth-Sci. Rev.* **12,** 1–33.
Taylor, S. R., 1980. Refractory and moderately volatile elements in the earth, moon and meteorites. *Proc. Lunar and Planetary Sci. Conf.* **11,** 333–48.
Thompson, R. N., Morrison, M. A., Dickin, A. P., & Hendry, G. L., 1983. Continental flood basalts . . . arachnids rule OK? In: Hawkesworth, C. J., & Norry, M. J. (eds.) *Continental Basalts and Mantle Xenoliths.* Nantwich, Cheshire: Shiva, 158–85.
———Hendry, G. L., & Parry, S. J., 1984. An assessment of the relative roles of crust and mantle in magma genesis: an elemental approach. *Philos. Trans. R. Soc. Lond.*, **A310,** 549–90.
Upton, B. G. J., 1987. Gabbroic, syenogabbroic and syenitic cumulates of the Tugtutoq younger giant dyke complex, south Greenland. In: Parsons, I. (ed.) *Origins of Igneous Layering.* Dordrecht: D. Reidel, 93–123.
——Emeleus, C. H., 1987. Mid-Proterozoic alkaline magmatism in southern Greenland: the Gardar province. In: Fitton, J. G., & Upton, B. G. J. (eds.) *Alkaline Igneous Rocks. Geol. Soc. Spec. Publ.* **30,** 449–71.
Williams, H., Turner, F. J., & Gilbert, C. M., 1982. *Petrography: An Introduction to the Study of Rocks in Thin Sections, 2nd Edn.* New York: Freeman, 626 pp.
Wilson, A. H., 1982. The geology of the Great 'Dyke', Zimbabwe: the ultramafic rocks. *J. Petrology* **23,** 240–92.
Winchester, J. A., & Floyd, P. A., 1977. Geochemical discrimination of different magma series and their differentiation products using immobile elements. *Chem. Geol.* **20,** 325–43.
Windley, B. F., 1986. Comparative tectonics of the western Grenville and the western Himalaya. In: Moore, J. M., Davidson, A., & Baer, A. J. (eds.) *The Grenville Province Geol. Assoc. Canada Spec. Paper* **31,** 341–8.
Wood, B. J., 1976. An olivine–clinopyroxene geothermometer. *Contr. Miner. Petrol.* **56,** 297–303.
York, D., 1966. Least-squares fitting of a straight line. *Can. J. Earth Sci.* **44,** 1079–86.